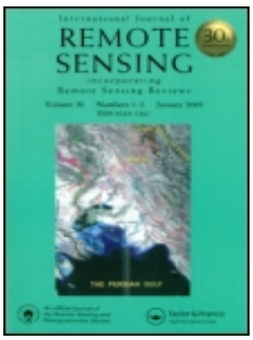

International Journal of Remote Sensing

ISSN: 0143-1161 (Print) 1366-5901 (Online) Journal homepage: http://www.tandfonline.com/loi/tres20

Finer resolution observation and monitoring of global land cover: first mapping results with Landsat TM and ETM+ data

Peng Gong , Jie Wang , Le Yu , Yongchao Zhao , Yuanyuan Zhao , Lu Liang , Zhenguo Niu , Xiaomeng Huang , Haohuan Fu , Shuang Liu , Congcong Li , Xueyan Li , Wei Fu , Caixia Liu , Yue Xu , Xiaoyi Wang , Qu Cheng , Luanyun Hu , Wenbo Yao , Han Zhang , Peng Zhu , Ziying Zhao , Haiying Zhang , Yaomin Zheng , Luyan Ji , Yawen Zhang , Han Chen , An Yan , Jianhong Guo , Liang Yu , Lei Wang , Xiaojun Liu , Tingting Shi , Menghua Zhu , Yanlei Chen , Guangwen Yang , Ping Tang , Bing Xu , Chandra Giri , Nicholas Clinton , Zhiliang Zhu , Jin Chen & Jun Chen

To cite this article: Peng Gong , Jie Wang , Le Yu , Yongchao Zhao , Yuanyuan Zhao , Lu Liang , Zhenguo Niu , Xiaomeng Huang , Haohuan Fu , Shuang Liu , Congcong Li , Xueyan Li , Wei Fu , Caixia Liu , Yue Xu , Xiaoyi Wang , Qu Cheng , Luanyun Hu , Wenbo Yao , Han Zhang , Peng Zhu , Ziying Zhao , Haiying Zhang , Yaomin Zheng , Luyan Ji , Yawen Zhang , Han Chen , An Yan , Jianhong Guo , Liang Yu , Lei Wang , Xiaojun Liu , Tingting Shi , Menghua Zhu , Yanlei Chen , Guangwen Yang , Ping Tang , Bing Xu , Chandra Giri , Nicholas Clinton , Zhiliang Zhu , Jin Chen & Jun Chen (2013) Finer resolution observation and monitoring of global land cover: first mapping results with Landsat TM and ETM+ data, International Journal of Remote Sensing, 34:7, 2607-2654, DOI: 10.1080/01431161.2012.748992

To link to this article: http://dx.doi.org/10.1080/01431161.2012.748992

International Journal of Remote Sensing
Vol. 34, No. 7, 10 April 2013, 2607–2654

Taylor & Francis
Taylor & Francis Group

Finer resolution observation and monitoring of global land cover: first mapping results with Landsat TM and ETM+ data

Peng Gong[a,b,c]*, Jie Wang[c], Le Yu[a], Yongchao Zhao[d,e], Yuanyuan Zhao[a], Lu Liang[b], Zhenguo Niu[c], Xiaomeng Huang[a], Haohuan Fu[a], Shuang Liu[c], Congcong Li[f], Xueyan Li[f], Wei Fu[c], Caixia Liu[c], Yue Xu[f], Xiaoyi Wang[c], Qu Cheng[a], Luanyun Hu[a], Wenbo Yao[a], Han Zhang[a], Peng Zhu[c], Ziying Zhao[f], Haiying Zhang[c], Yaomin Zheng[c], Luyan Ji[e], Yawen Zhang[g], Han Chen[g], An Yan[g], Jianhong Guo[h], Liang Yu[h], Lei Wang[c], Xiaojun Liu[g], Tingting Shi[g], Menghua Zhu[g], Yanlei Chen[b], Guangwen Yang[a], Ping Tang[c], Bing Xu[f], Chandra Giri[i], Nicholas Clinton[a], Zhiliang Zhu[i], Jin Chen[j], and Jun Chen[k]

[a]Ministry of Education Key Laboratory for Earth System Modelling, Centre for Earth System Science, Tsinghua University, Beijing 100084, China; [b]Department of Environmental Science, Policy and Management, University of California, Berkeley, CA 94720-3114, USA; [c]State Key Laboratory of Remote Sensing Science, Jointly Sponsored by Institute of Remote Sensing Applications, Chinese Academy of Sciences, and Beijing Normal University, Beijing 100101, China; [d]Department of Geography, University of South Florida, Tempa, FL 33620, USA; [e]Institute of Electronics, Chinese Academy of Sciences, Beijing 100191, China; [f]College of Global Change and Earth System Science, Beijing Normal University, Beijing 100875, China; [g]College of Remote Sensing Information Engineering, Wuhan University, Wuhan 430072, China; [h]Beijing Xiuying Environmental Information Technology Development Inc., Beijing 100101, China; [i]United States Geological Survey, Reston, VA 12201, USA; [j]State Key Laboratory of Earth Surface Processes and Resource Ecology, Beijing Normal University, Beijing 100875, China; [k]National Geomatics Centre, Beijing 100830, China

(*Received 23 October 2012; accepted 1 November 2012*)

We have produced the first 30 m resolution global land-cover maps using Landsat Thematic Mapper (TM) and Enhanced Thematic Mapper Plus (ETM+) data. We have classified over 6600 scenes of Landsat TM data after 2006, and over 2300 scenes of Landsat TM and ETM+ data before 2006, all selected from the green season. These images cover most of the world's land surface except Antarctica and Greenland. Most of these images came from the United States Geological Survey in level L1T (orthorectified). Four classifiers that were freely available were employed, including the conventional maximum likelihood classifier (MLC), J4.8 decision tree classifier, Random Forest (RF) classifier and support vector machine (SVM) classifier. A total of 91,433 training samples were collected by traversing each scene and finding the most representative and homogeneous samples. A total of 38,664 test samples were collected at preset, fixed locations based on a globally systematic unaligned sampling strategy. Two software tools, Global Analyst and Global Mapper developed by extending the functionality of Google Earth, were used in developing the training and test sample databases by referencing the Moderate Resolution Imaging Spectroradiometer enhanced vegetation index (MODIS EVI) time series for 2010 and high resolution images from Google Earth. A unique land-cover classification system was developed that can be crosswalked to the existing United Nations Food and Agriculture Organization (FAO)

*Corresponding author. Email: penggong@berkeley.edu

ISSN 0143-1161 print/ISSN 1366-5901 online

http://dx.doi.org/10.1080/01431161.2012.748992
http://www.tandfonline.com

land-cover classification system as well as the International Geosphere-Biosphere Programme (IGBP) system. Using the four classification algorithms, we obtained the initial set of global land-cover maps. The SVM produced the highest overall classification accuracy (OCA) of 64.9% assessed with our test samples, with RF (59.8%), J4.8 (57.9%), and MLC (53.9%) ranked from the second to the fourth. We also estimated the OCAs using a subset of our test samples (8629) each of which represented a homogeneous area greater than 500 m × 500 m. Using this subset, we found the OCA for the SVM to be 71.5%. As a consistent source for estimating the coverage of global land-cover types in the world, estimation from the test samples shows that only 6.90% of the world is planted for agricultural production. The total area of cropland is 11.51% if unplanted croplands are included. The forests, grasslands, and shrublands cover 28.35%, 13.37%, and 11.49% of the world, respectively. The impervious surface covers only 0.66% of the world. Inland waterbodies, barren lands, and snow and ice cover 3.56%, 16.51%, and 12.81% of the world, respectively.

1. Introduction

Global land-cover data are key sources of information for understanding the complex interactions between human activities and global change (Running 2008). Land-cover data are some of the most important variables in all nine societal benefit areas that the Global Earth Observation System brings (Herold et al. 2008). They are also some of the most critical variables for climate change studies (Bounoua et al. 2002; Ge et al. 2007; Hibbard et al. 2010; Imaoka et al. 2010). Land-cover data products play a critical role in improving performances of ecosystem, hydrologic, and atmospheric models (Tucker, Townshend, and Goff 1985; Bounuoa et al. 2002; Foley et al. 2005; Jung et al. 2006). They are also essential to studies of habitat and biodiversity (Buchanan et al. 2008; Hall et al. 2011), carbon cycling (de Moraes et al. 1998; DeFries, Houghton, and Hansen 2002; Ganzeveld et al. 2011; Liu et al. 2011; Poulter et al. 2011), and public health (Xu et al. 2004; Liang et al. 2010).

Six types of global land-cover maps derived from remotely sensed data are freely available at 1 km and 300 m scales.

- The 1 km International Geosphere-Biosphere Programme Data and Information System Cover (IGBP-DISCover) map was produced from monthly normalized difference vegetation index (NDVI) composites derived from 1992 to 1993 National Oceanic and Atmospheric Administration (NOAA) Advanced Very High Resolution Radiometer (AVHRR) data (Loveland et al. 2000). An unsupervised classification method was used to produce this map.
- The 1 km University of Maryland (UMD) land-cover map was produced with the same data set as mentioned above (Hansen et al. 2000). A supervised classification tree method was used to produce this map.
- The 1 km Global Land Cover 2000 (GLC2000) map was produced from monthly NDVI data derived from 1999 to 2000 Satellite Pour l'Observation de la Terre (SPOT) vegetation data (Bartholome and Belward 2005). It was produced by people working separately, in parallel, on 19 different regions of the world using various types of algorithms.
- 500 m Moderate Resolution Imaging Spectrometer (MODIS) land-cover maps are now being generated annually with MODIS data (Friedl et al. 2002, 2010). Recently, a supervised classification tree algorithm has been used to produce these maps.
- 300 m GlobCover land-cover maps were produced with bimonthly Medium Revolution Imaging Spectrometer (MERIS) data mosaics derived from the Environmental Satellite (ENVISAT) for 2005 and 2009 (Arino et al. 2008; Bontemps

et al. 2010). They were produced with an automatic multi-stage classification procedure using spectral–temporal and phenological information with an unsupervised classification method.

- The 1 km MODIS land-cover map was derived from the MODIS 1 km monthly product led by Japan through international collaboration (Tateishi et al. 2011). A combination of supervised classification and single-class extraction algorithms was used to make this map.

The classification schemes used by the three US global land cover products (IGBP-DISCover, UMD, MODIS) used the IGBP classification system with 17 categories of cover types, whereas the two European products (GLC2000, GlobCover) used a 22 category classification scheme that was developed for similar purposes by the IGBP system in order to meet global modelling purposes. This has come about through a standard class definition and aggregation system developed by the Food and Agriculture Organization (FAO) (Di Gregorio 2005). All land-cover products were generated by computer classification algorithms of different types but on a per-pixel basis. The overall accuracy (OA) of the IGBP DISCover map was 66.9% (Scepan 1999), and the GLC2000 map was 68.6% (Mayaux et al. 2006). Cross-validated OA (using training data) for the MODIS product was 78.3% (Friedl et al. 2002) and 77.9% for GlobCover based on 2186 random samples of homogeneous land covers (Arino et al. 2008). Through international collaboration, Tateishi et al. (2011) made use of reference map data from over 180 countries. They developed their own classification scheme with 20 classes. Using a validation data set of 600 points, they reported an OA of 76.5%.

In spite of these validation assessments, some third-party researchers have found considerably lower accuracies in different parts of the world when verifying the various global land-cover products (Gong 2009a; Fritz, See, and Rembold 2010). Using 400 field survey points to assess the MODIS land-cover product, Sedano, Gong, and Ferrao (2005) found greater than 50% error in the Mozambique Miombo ecosystem over an area of approximately 100,000 km^2. Using over 2000 field samples collected in Siberia covering approximately 1 million km^2, Frey and Smith (2007) found that the OAs for the IGBP DisCover and MODIS global land-cover products were 22% and 11%, respectively. From a global comparison of the IGBP DISCover, UMD, MODIS, and GLC2000 data products, it was found that relatively consistent results can be found only over the snow and ice fields of Greenland, the desert areas in Africa, and the rain-forests of the Amazon Basin, areas occupying 26% of the global land surface (MaCallum et al. 2006). From seven selected 500 km $\times$ 500 km comparison areas, in Africa, Asia, Australia, Europe, North America, Russia, and South America, the consistencies among these four global land-cover products for all but South America were below 20%. Using 250 Fluxnet sites, Gong (2009a) found that the OAs of the first three global land-cover maps produced with the IGBP classification system were below 42%. Previous research found that accuracies for different land-cover categories varied greatly, with evergreen broadleaf forest and desert areas best classified, but heterogeneous land-cover areas poorly classified (Jung et al. 2006; Herold et al. 2008).

It seems that so far only the evergreen broadleaf and the snow and ice cover classes have been reliably mapped with certainty. Mixed trees, deciduous broadleaf trees, shrub, and herbaceous land covers are the most confused classes (Herold et al. 2008; Sterling and Ducharne 2008). A spatial consistency check revealed that tropical forest, barren, and snow and ice cover classes are mapped homogeneously, but many transitional zones have low classification accuracies where finer resolution data are called for (Herold et al. 2008; Tchuente, Roujean, and de Jong 2011). It was believed that '. . . improving the mapping

of heterogeneous landscapes is the most significant challenge for improving global land-cover mapping. Future efforts based on finer resolution data may provide improvements' (Herold et al. 2008). However, this does not come without significant costs for data, local knowledge, and detailed field data.

Current trends in land-cover classification have shifted from a single general purpose classification to individual class information extraction for human settlements (Imhoff 1997; Lu et al. 2008; Schneider et al. 2010; Wang et al. 2010), agricultural lands (Ramankutty and Foley 1998, 1999; Thenkabail et al. 2009), wetlands (Niu et al. 2009; Giri et al. 2010; Gong et al. 2010), lakes (Sheng, Shah, and Smith 2008), wildland fires (Pu et al. 2007; Chuvieco, Giglio, and Justice 2008), and quantification of vegetation cover fractions (DeFries, TownShend, and Hansen 1999; Hansen, DeFries, and Townshend 2002; Clinton et al. 2009). In addition, classification algorithms have increased from simple statistical classifiers like the widely used maximum likelihood classifier (MLC), to classification trees (such as the seminal CART and C4.5) to more computationally demanding machine-learning classifiers such as support vector machines (SVM) and ensemble classifiers such as Random Forest (RF), and other bagged or boosted classifiers (Witten and Frank 2005). Due to the improvement of computational efficiency, it is now easier to employ and compare results from a number of different classifiers in a mapping task (e.g. Carreiras, Preira, and Shima bukuro 2006; Clinton et al. 2009). In the meantime, more and more ancillary information and remotely sensed data from different sources are being used in land-cover classification (e.g. Aksoy et al. 2009). From a global perspective, data provided for browsing purposes in virtual globes, particularly Google Earth, have proved useful for their geometric precision and large volumes of high spatial resolution data available at better than 1 m level (Yu and Gong 2012).

In summary, existing global land-cover maps derived from remote sensing were all based on time series of coarser resolution satellite data. The time series is usually for a specific year. Recent advances in data acquisition, data accessibility, and high-performance computing make it possible to use finer spatial resolution data for global land-cover mapping. In particular, as more Landsat-level data are made freely accessible, it is natural to consider adopting such medium resolution data for global land-cover mapping purposes. Although it is still hard to collect medium resolution data for the entire globe in a consistent season or a year, it is possible to use such data in multiple years to cover the entire globe. Townshend et al. (2012) reported their efforts in mapping global forest cover and monitoring forest changes using Landsat data. They found that atmospheric interference, terrain effects, selecting data from the appropriate season in a year, and training sample selection are particularly challenging.

Despite these difficulties, globally consistent land-cover data from medium resolution satellite sensors that are an order of magnitude finer than weather satellite sensors have never been produced, but they are badly needed for many reasons. First, land process models at regional and global scales need better surface cover fraction data that coarser resolution data cannot provide. Second, although land-cover data at the medium resolution exist, in many developed countries, their classification schemes vary widely making them hard to crosswalk for cross-regional studies such as water resources management in international river basins, conservation of wildlife and biodiversity, and carbon sequestration planning through afforestation. This requires a global land-cover map with a consistent land-cover classification scheme. Third, many developing countries in Africa and Asia do not have land-cover data at this scale. A global land-cover map can fill this gap.

In this article, we report our first efforts in mapping global land cover with 30 m resolution Landsat Thematic Mapper (TM) and Enhanced TM plus (ETM+) data. This was

carried out under our Finer Resolution Observation and Monitoring of Global Land Cover (FROM-GLC) project. Our long-term goal in FROM-GLC is to develop a multiple stage approach to mapping global land cover so that the results can better meet the needs of land process modelling and other application needs mentioned earlier that global land-cover maps produced with coarser resolution data failed to meet. The FROM-GLC project should also be easily crosswalkable to existing global land-cover classification schemes. Presented here is our first step that maps broad land-cover categories based on spectral data only. It is meant to serve as a benchmark for future improvements when spatial and temporal and other ancillary features are combined. As Landsat-like data are being made more frequently available, optimal dates for data selection and multiseasonal data in the same year cannot be used in the future. Future improvements can be expected based on alternative algorithms such as object-based image classification and selection of data from more suitable seasons and atmospheric conditions, and use of multitemporal scenes and new features including vegetation fraction estimated from Landsat-class data, as well as other information extracted from other sources such as vegetation height, biogeographical modelling, and analysis of terrain and climate data.

2. Data pre-processing and image classification procedure

A total of 8929 Landsat TM/ETM+ scenes were collected from various sources (Figures 1 and 2). A total of 2181 scenes were collected from the Global Land Cover Facility (GLCF) at the UMD, 6229 scenes were collected from United States Geological Survey (USGS) Earth Resources Observation and Science (EROS) data centre, and an additional 519 scenes were collected from the Satellite Ground Station of China. About 74% of the imagery was acquired after 2006, while images available before 2006 were used as substitutes for places where no suitable imagery could be found after 2006 at the time of the project initiation. Only 18 scenes acquired before 1998 were used. As a result, approximately three quarters of the imagery is circa 2010 and one quarter is circa 2000. Most of the scenes except those covering China were processed to level L1T (orthorectified), while 161 scenes at higher latitudes were processed to level L1G (non-orthorectified, Figure 3). Only geometrical correction was applied to the images covering China. Since the non-orthorectified images were mainly taken over relatively flat areas, terrain effects were considered negligible where orthorectified imagery was unavailable. A total of 40 scenes were randomly

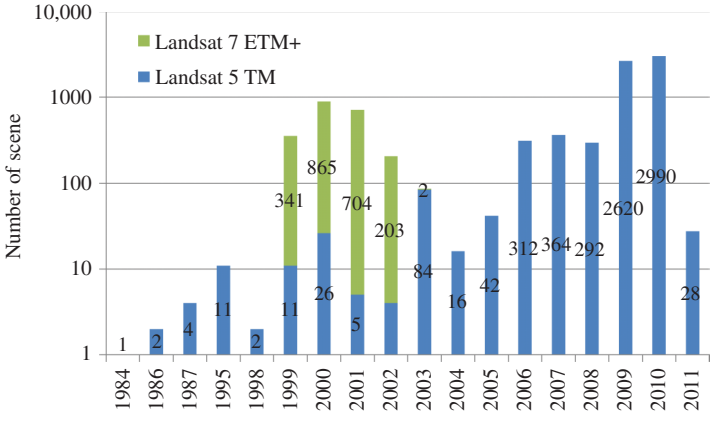

Figure 1. The temporal distribution of Landsat scenes used in this study ($N = 8929$).

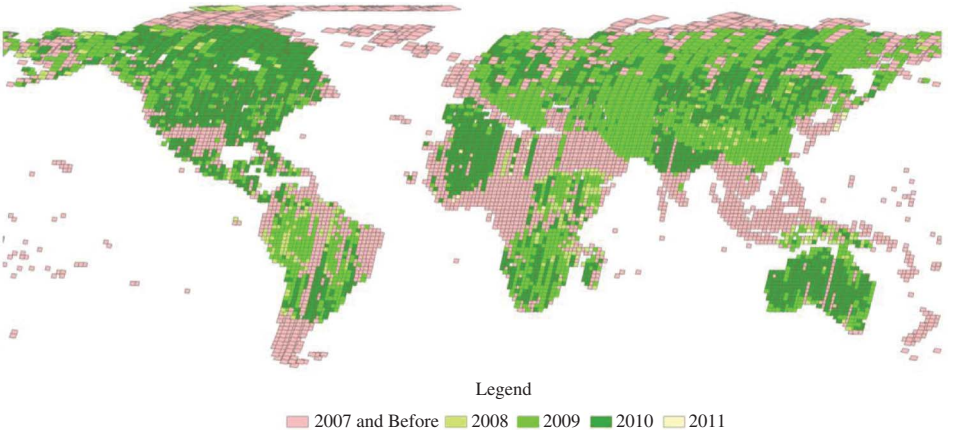

(*a*)

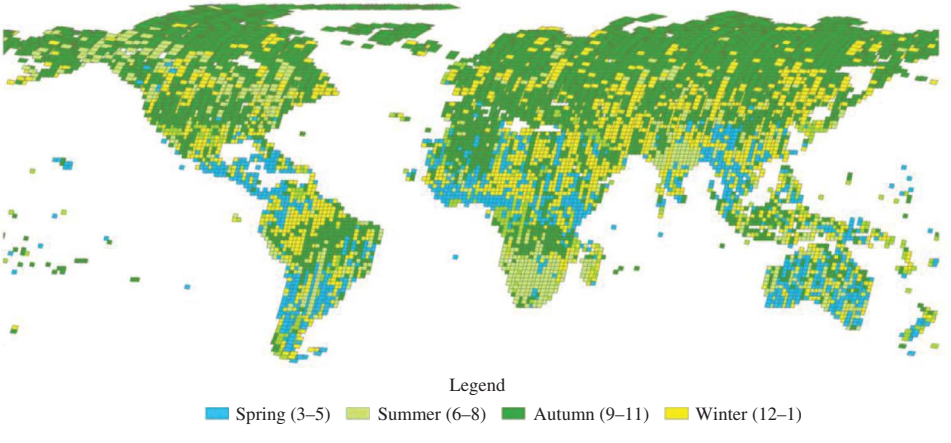

(*b*)

Figure 2. Temporal distribution of Landsat scenes used in this study. Annual distributions (*a*) and seasonal distribution (*b*) of scenes.

Figure 3. Processing level distributions. Levels L1T (brown) and L1G (blue).

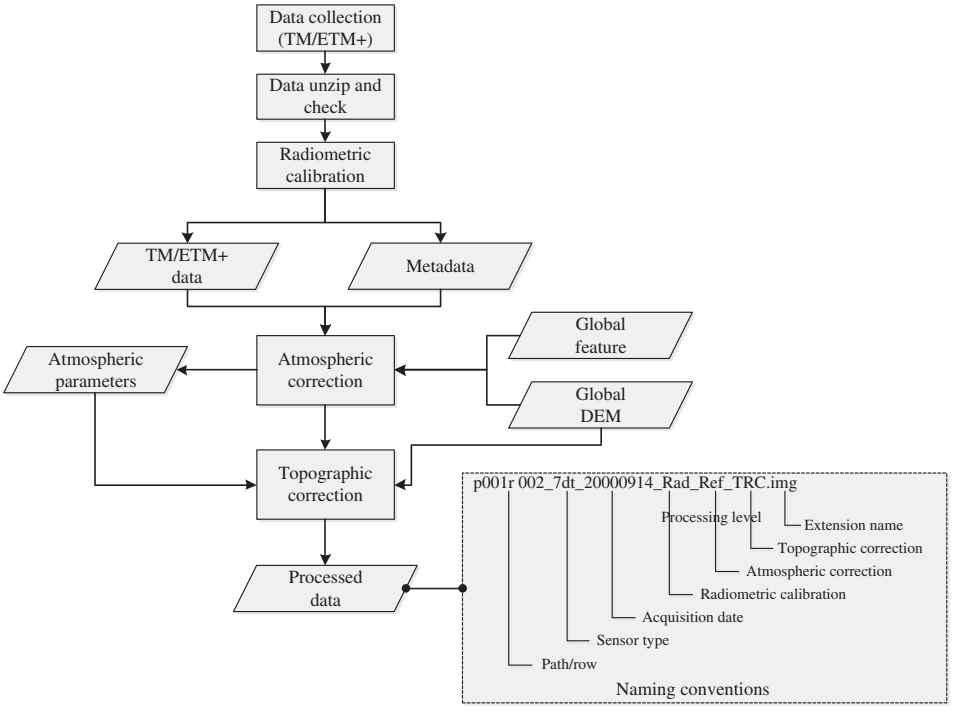

Figure 4. Radiometric processing of Landsat TM and ETM+ scenes.

selected to evaluate the geometric discrepancy against Google Earth images. In each scene, we selected 10 ground control points from typical locations to calculate a root mean square error (RMSE). We found that only one scene in Russia near the Arctic had an RMSE of 2.76 pixels. The remaining RMSEs were below 1.43 pixels. On average, the RMSE was 1.01 pixels, indicating an acceptable geometric agreement between the Landsat images and Google Earth images.

Except those images from the GLCF that were already radiometrically corrected to reduce atmospheric and topographic effects, all remaining L1T images from USGS were radiometrically corrected with our own software (Figure 4).

The overall work flow of our global land-cover classification is shown in Figure 5. It involves data pre-processing, training, and test sample collection, image classification on a scene-by-scene basis using local training samples from spatio-temporal neighbourhood scenes, and finally accuracy assessment.

The radiometric processing was done automatically using the Global Mapper (GM) software package developed by ourselves. This processing includes atmospheric correction and topographic correction. The final product is images of reflectance with the atmospheric and topographic effects substantially reduced. After automatic processing, manual checking was carried out to ensure correction quality. Scenes with a poor quality correction were re-processed with manually selected parameter sets.

Atmospheric correction was done with an enhanced version of the Fast Line-of-Sight Atmospheric Analysis of Spectral Hypercubes (FLAASH) algorithm (Alder-Golden et al. 1999) implemented in the GM (see Section 3). Parameter setup was automatically generated based on the acquisition time and location information from the imagery and ancillary data.

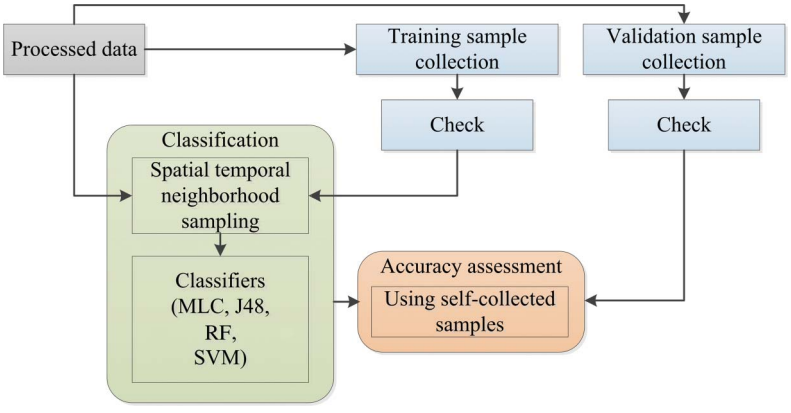

Figure 5. Classification workflow.

For example, the elevation information was obtained from the Geospatial Image Pyramid (GIP) of the global digital elevation model (DEM) data (recognizable by Google Earth and Environment for Visualizing Images (ENVI)). Aerosol data are inferred from the location information of each scene and DEM data. The GM FLAASH module also contains an automatic processing and optimization mechanism. When it detects over-correction of the imagery, indicated by a large quantity of 0 values, it automatically adjusts the water vapour, and aerosol parameters, feeding the optimized parameters back into the atmospheric correction. After the atmospheric correction, the optimized parameters are recycled for use by the topographic correction procedure.

The topographic correction is based on the TopoRadCor procedure in GM. TopoRadCor takes the output from the atmospheric correction and uses the 90 m DEM from the GIP as input. The solar incidence angle is computed based on the DEM and the location and local time information for each pixel. The topographic correction can reduce the distortion over higher latitudes and complex terrain. TopoRadCor automatically adjusts to surface cover type, resulting in a well-characterized surface structure that overcomes over-correction effects (Figure 6).

Although we tried to collect as many processed scenes as we could, by the time of training and test sample collection, there were still 656,889 km^2 of terrestrial land areas

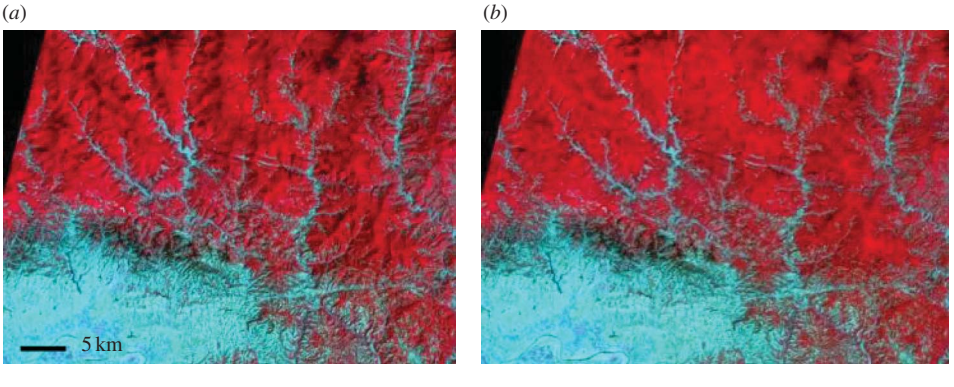

Figure 6. Effect of TopoRadCor process. (*a*) The original image (Location: Shaanxi, China; centre latitude 33° 22′ 2.40″ N, centre longitude 107° 45′ 20.31″ E) and (*b*) The resultant image.

(excluding Antarctica and Greenland) not covered by our images. These areas were mostly distributed within the Arctic region. Canada, the USA, Russia, and Norway (Svalbard) were among the top four countries with the largest un-mapped areas. Among the 8929 scenes used in this project, 192 scenes were sampled twice by different interpreters due to overlaps in separate national and continental mapping task assignments. A total of 1007 scenes (including those 192 scenes mentioned above) share the same Path/Row collected at different times. Training samples were collected on all these images resulting in higher sample density over those overlap areas.

We experimented with four types of classifiers: the traditional MLC, a simple J4.8 decision tree classifier (an improved version of C4.5), support vector machine (SVM) classifier, and RF classifier (Bradski 2000; Hall et al. 2009; Chang and Lin 2011). The MLC was used as a reference for its popularity, computational simplicity, and robustness. Recently, The SVM classifier has been widely reported as an outstanding classifier in remote sensing (Huang, Davis, and Townshend 2002; Liu, Kelly, and Gong 2006). The RF classifier was tested due to its reported performance in the machine learning community (Bauer and Kohavi 1999; Caruna and Niculescu-Mizil 2006). The parameter set used in this study for each of the classifiers is listed in Table 1.

Representative sample collection is the most time-consuming and labour-intensive process in the global land-cover mapping effort. Limited by human power, we could not collect as many training samples as we would have liked for each class in every scene. We used samples collected in neighbouring scenes to augment training samples. Training samples collected from any particular scene were pooled with samples from a certain number of neighbouring scenes and were used to train a classifier for that particular scene. This is not usually needed in training sample collection when mapping areas are smaller in size but is considered to be a necessary alternative for global mapping. The selection rule is set to be 30 neighbouring scenes that meet the spatial and temporal criteria. The search for spatial neighbour images is limited within each of the ecoregions as defined by the World Wildlife Fund (Olson et al. 2001). Temporal neighbour images are based on the acquisition date of images. At first, image acquisition time is $\pm$ 30 days from the current image. If 30 neighbourhood scenes cannot be found, the time is relaxed to $\pm$ 60 days. If 30 neighbourhood

Table 1. Classification algorithms and parameter settings.

Classifiers	Implementation	Parameters	Remarks
MLC	OpenCV	Default	Naïve/normal Bayes classifier
RF	WEKA	Calculate the variable importance of each feature during training: true Size of the randomly selected subset of features to be tested at any given node: 2 Maximum tree count: 50	
J4.8	WEKA	Minimum number of object per leaf: 2 Confidence factor for pruning: 0.1 Unpruned: false	
SVM	LibSVM	Kernel: RBF *C* (cost): 100 gamma: 0.1 Probability estimates: false	Data were scaled to [0, 1] before training and classification

Note: RBF, radial basis function.

scenes are still not available, the time is further relaxed to ± 90 days. If still 30 neighbourhood scenes cannot be found, use what is available. All bands except the thermal band of the TM or ETM+ images were used in the classification.

All image classification tasks were done on the supercomputer at Tsinghua University. The total disk space of this supercomputer exceeds 1000 TB. The system has 740 nodes, each of which is equipped with 2 Intel Xeon X5670 CPU (6 Kernels, 2.93 GHz, 12 MB Cache) and 32–48 GB of memory. Our application employed less than 1.5 GB memory in each kernel and less than 18 GB for each node. The total volume of our data input to the supercomputer is 3 TB, and our total output data volume is approximately 2.5 TB. A maximum of 1200 cores was used for any one part of the processing. The parallelization scheme for running the classification on the supercomputer is straightforward. An approximately equal number of scenes is assigned to each core, and their processing results are stored on a scene-by-scene basis. With 1200 cores, it takes approximately 6 days to complete the SVM classification of all images. If all cores are used on this supercomputer, the classification task can be done within a day for the entire world. The low computation efficiency of the SVM is the major reason for us to use the parallel computer.

3. Global mapping software development

In order to support global land-cover mapping and analysis, we developed software to expand the image processing and spatial data analysis functionality in Google Earth (Gong et al. 2011; Yu and Gong 2012). Basic functions commonly found in geographic information system (GIS) software packages for data editing, spatial database development, and map overlay are included in the software package, Global Analyst (GA) (http://www.globalanalyst.cn/ga2/index.html). GA is a GIS, based on a spherical coordinate system, that encapsulates Google Earth. GA integrates the functions from two different systems (GIS and remote sensing (RS)) and adopts advanced software technologies such as cloud computing, scalable architecture, and multilingual hybrid programming. In GA, globally distributed multisource, multiscale, multitemporal geospatial (e.g. shp., and tif.) data and services (e.g. WMS, WCS, and WFS) can be aggregated or mashed-up. Customized functions for particular applications can be added into GA with JavaScript.

To handle arbitrary images in addition to those provided in Google Earth, we developed a software package GM that enables image processing coupled with Google Earth image display and visualization. When an image processing task starts, it not only opens the image but also opens Google Earth and automatically synchronizes the two by their locations. This along with GA has greatly improved the efficiency of training and test sample collection (Figure 7).

4. Classification system design

Existing global land-cover maps were produced for different purposes from different types of data with different types of algorithms. Some were developed by different groups of creators. Their classification schemes and implementations are also inconsistent. As a result, a thorough comparison of different land-cover maps is challenging if not impossible. Even so, some efforts have been made to crosswalk and compare these results (Herold et al. 2008; Tateishi et al. 2011).

Based on the analysis of existing classification systems, we found that there are major limitations to using a composite class type that combines vegetation trait, structure, and life-form information in a fixed manner. Taking the IGBP, GLC2000, and GLOBCover classification systems as examples, although the three systems differ in some details, they

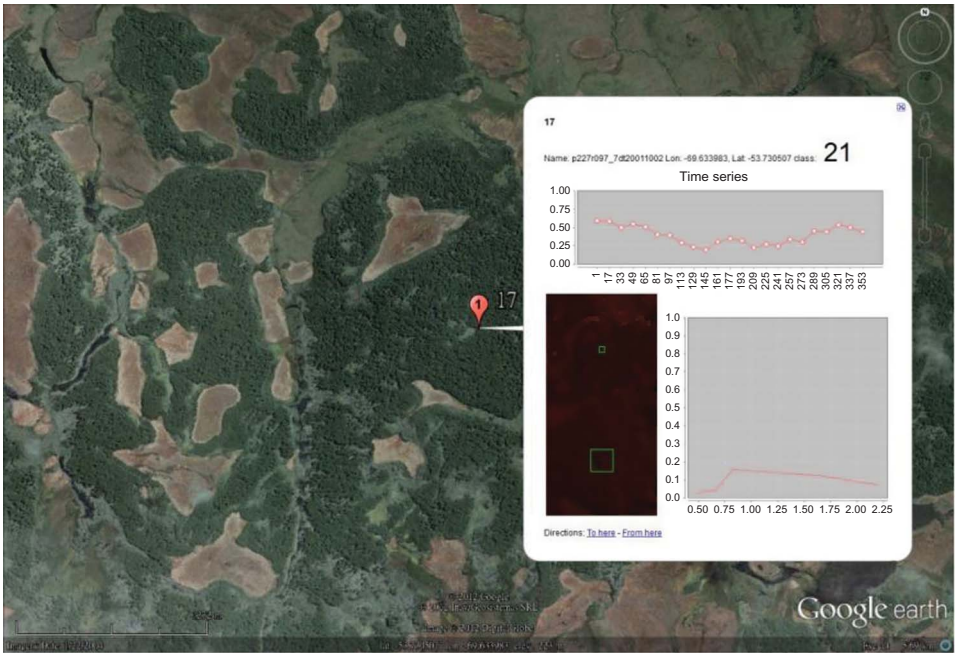

Figure 7. Test sample identification with a pre-determined sample location. The background is Google Earth image with TM image, the spectral curve, and the MODIS time-series vegetation index curve shown in the pop-up box.

have high consistency as well. All vegetation categories contain life form, canopy closure, and height specifications, but different thresholds within a category. The IGBP system specifies that woody vegetation under 2 m height is classified as shrubs whereas the height limit was increased to 3 m in the GLC2000 and 5 m in the GlobCover classification systems. Similarly, the canopy closure in different vegetation classes varied among the classification systems. Most land-cover classification systems do not include the distinction between C3 and C4 photosynthetic types but they are needed for land surface process models (DeFries et al. 1995; Dai et al. 2003). However, such information is hard to obtain from remotely sensed data. Additional data sources or biogeographical modelling results are often considered for obtaining such information (Stirling and Ducharne 2008).

In our design, we chose to build a system separating the trait, life form, and structural information into distinct layers, retaining the original quantitative structural information as much as possible. We treat traits, life form, and structural data as basic building blocks towards the construction of a complete classification system. We call these building blocks end-components. Table 2 lists the level 1 land-cover categories of GlobCover with a decomposition of its classes into end-components. From Table 2, it can be seen that a composite class can be defined in terms of four types of end-components: cover type, life form or plant functional type (PFT), canopy or crown closure, and height. Through a decomposition analysis, most complicated land-cover classification systems can be divided into simplified end-component classes. There are a total of 10 land-cover types and eight life form or PFT classes. Canopy closure and heights can be preserved in unclassified form in their original quantities. As we de-coupled the nominal cover-type end-component from canopy closure and height end-components that can be quantitatively characterized, we were able to define

Table 2. A decomposition of the GlobCover land-cover classes into end-components.

Code	Description of composite classes	Cover type	Form/PFT	Closure (%)	Height (m)
11	Post flooding or irrigated cr	Cropland	C3/C4		
14	Rainfed croplands	Cropland	C3/C4		
20	Mosaic cropland/vege	Crop/vege	C3/C4	50–70	
30	Mosaic vege/cropland	Crop/vege	C3/C4	50–70	
40	>15%-BL-EG/Semi DFo>5 m	Forest	BL EG/D	>15	>5
50	>40% BL D Fo>5 m	Forest	BL D	>40	>5
60	15–40% BL D Fo>5 m	Forest	BL D	15–40	>5
70	>40% NL EG Fo>5 m	Forest	NL EG	>40	>5
90	15–40% NL D EG Fo>5 m	Forest	BL D/EG	15–40	>5
100	>15% ML Fo>5 m	Forest	BL/NL	>15	>5
110	MoFo/Sh(50–70%)/G (20–50)	Fo/shrub/grass	C3/C4	50–70	
120	MoG(50–70)/F/Sh(20–50)	Fo/shr/grass	C3/C4	50–70	
130	>15% Sh(<5 m)	Shr	C3/C4	>15	<5
140	>15% G	Grassland	C3/C4	>15	
150	<15% Vege	Vege	C3/C4	<15	
160	>40% BL FoRegFl Fresh	Inland fowetl	BL	>40	
170	>40% semi BL EG regFl Sal	Coastal fowetl	BL semi D/EG	>40	
180	>15% vege on regFl or w log	Marshland	Watered veg/ C3/C4	>15	
190	Artificial (urban > 50%)	Urban		>50	
200	Bare	Bare	Wd/Wt form		
210	Water	Water			
220	Permanent snow/ice	Snow/ice			

mixture land-cover classes more precisely than previous land-cover classification systems. We can resolve any land-cover class in a new classification system that contains those quantitative end-components. In fact, different types of end-components should be derived from different sources of data or by different types of algorithms. For example, the canopy closure can be derived by applying linear unmixing or regression techniques (Gong, Miller, and Spanner 1994; Roberts et al. 1998; Hansen, DeFries, and Townshend 2002) to the spectral data, whereas vegetation height information can be obtained from other sources of data such as stereo pairs of images (Gong 2002), interferometry of synthetic aperture radar (SAR) data (Neumann, Ferro-Famil, and Reigber 2010), or the use of lidar data (Lefsky 2010; Hall et al. 2011; Simard et al. 2011). We argue that future classification systems should be separately designed for different types of end-components. This will make such systems easily crosswalkable to existing classification systems using an end-component and layered approach.

Based on the end-component analysis and the potential of only six bands of spectral data from TM and ETM+ imagery, we targeted the determination of the cover-type end-component at this initial stage of global land-cover mapping. In addition, we included some life form categories spectrally separable from the TM data such as broadleaved and coniferous trees (at level 2). The resultant classification scheme, with a two-level hierarchy involving only the cover-type end-component, is listed in Table 3.

Table 3. Land-cover types used in this study.

Level 1	Level 2	LCC label	Group	LCC level	LCC code	Description	Translation notes
10 Croplands						This type of land has clear traits of intensive human activity. It varies a lot from bare field, seeding, crop growing to harvesting. It can be easily identified if edges or textures are visible with sufficiently large land parcels. Fruit trees are classified into forests. Bare field is classified into bare land. Pasture could be transitional from croplands to natural grasslands.	
	11 Rice fields	Irrigated graminoid crops(s)	A11	A4XXXXC1D 3-S0308	11388-S0308	Land for rice cultivation.	
	12 Greenhouse farming					Land with plastic foam or grass roof protection with distinguishing spectral properties.	Hard to define 'Greenhouse framing' with LCCS
	13 Other croplands	Herbaceous crop(s)// Shrub crop(s)	A11//A11	A3//A2	10025//10013	This category includes arable and tillage land.	
20 Forest						Trees observable in the landscape from the images. Forest has a distinct canopy texture on TM images.	
	21 Broadleaf forests	Broadleaved closed to open trees	A12	A3A20B2XXD1	21495	Usually higher reflectivity than conifer species in the near infrared (NIR) spectral band. Shaded and sunlit sides less contrast.	LCCS limits tree cover percentage classification to >15%, limits tree height classification to >3 m
	22 Needleleaf forests	Needleleaved closed to open trees	A12	A3A20B2XXD1	21498	Lower reflectivity than broadleaf trees in the NIR band.	LCCS limits tree cover percentage classification to >15%, limits tree height classification to >3 m

(*Continued*)

Table 3. (*Continued*).

Level 1	Level 2	LCC label	Group	LCC level	LCC code	Description	Translation notes
	23 Mixed forests	Broadleaved Closed to open trees/ Needleleaved closed to open trees	A12	A3A20B2XX D1/A3A20B2 XXD1	21495/21498	Neither coniferous nor broadleaf trees dominate in a mixed forest stand.	LCCS limits tree cover percentage classification to >15%, limits tree height classification to >3 m
	24 Orchards	Tree Crop(s) Cover: Orchard(s)	A11	A1-W8	10001-W8	Parcels planted with fruit trees or shrubs: single or mixed fruit species, fruit trees associated with permanently grassed surfaces.	
30 Grasslands	31 Pastures	Herbaceous closed to open vegetation	A12	A6A10	20033	Grasslands for grazing.	LCCS limits herbaceous cover percentage classification to >15%
	32 Other grasslands	Herbaceous closed to open vegetation	A12	A6A10	20033	Natural grasslands identifiable.	LCCS limits herbaceous cover percentage classification to >15%
40 Shurblands		Closed to open shrubland (thicket)	A12	A4A20B3	21450	Shrub cover identifiable in the image. Has a texture finer than tree canopies but coarser than grasslands.	LCCS defines shrubland's height between 5 and 0.3 m, and cover percentage classification to >15%
50 Wetlands		Natural and semi-natural aquatic or regularly flooded vegetation	A24	A24	0007	Although wetland is defined in the RAMSAR convention to maximize wetland areas, we intend to include only marshland with distinctively high reflectivity in the NIR band. Low relief areas with perched bogs, playas, and patholes may also be included depending on the season of image acquisition time. Forested wetland is not included here as it cannot be well identified from TM images.	

	51 Marshland	Closed to open herbaceous vegetation/ closed to open lichens/ mosses	A24	A2A20/A7A20	42155/42260	Aquatic and hydrophytic herbaceous plants observable from the image as non-water cover.	LCCS limits vegetation cover to >15%
	52 Mudflats	Bare land/// river	B16///B28	A5///A1-A4	6005///8001-1	Generally unvegetated expanses of mud, sand or rock lying between high and low water lines.	
60 Waterbodies		Natural waterbodies/ artificial waterbodies	B28/B27	A1/A1	8001/7001	All inland waterbodies with >3 pixels in width or 8 pixel × 8 pixel (6 ha) in area. Patches of fish ponds are included in this category. Spectral characteristics vary widely and the waterbody change in area with season.	
	61 Lake	Natural waterbodies (standing)	B28	A1-A5	8001-5	Natural waterbodies.	
	62 Reservoir/ Pond	Artificial waterbodies	B27	A1-A5	7001-5	Dammed waterbodies.	
	63 River	Natural waterbodies (flowing)	B28	A1-A4	8001-1	Natural or artificial water-courses serving as water drainage channels. Minimum width for inclusion 3 pixels.	
	64 Ocean	Natural waterbodies: salinity	B28	A1B1-V2/ A1B1-V3/ A1B1-V4// A1B1-V5	8002-V2/8002-V3/8002-V4//8002-V5	Salinity water.	
70 Tundra		Closed to open lichens/mosses	A12	A7A20	21465	Located at high mountains above tree line and high latitude regions with low height vegetation. The growing season is between 1 and 2 months.	
	71 Shrub and Brush Tundra (= 40 Shrublands)					Dominated by low shrubs with grasses, lichens, and mosses at the background.	

(*Continued*)

Table 3. (*Continued*).

Level 1	Level 2	LCC label	Group	LCC level	LCC code	Description	Translation notes
	72 Herbaceous Tundra	Herbaceous closed to open vegetation //closed to open lichens/mosses	A11//A12	A2A20//A7A20	21453//21465	Dominated by various sedges, grasses, forbs, lichens, and mosses, all of which lack woody stems.	
80 Impervious		Artificial surfaces and associated area(s)	B15	A1/A2	5001/5004	Primarily based on artificial cover such as asphalts, concrete, sand and stone, bricks, glasses, and other cover materials.	
	81 Impervious-high albedo					Impervious road cover with high albedo materials (e.g. concrete, cement).	Hard to define 'Impervious-high albedo' with LCCS.
	82 Impervious-low albedo					Impervious roof tops covered by low albedo materials (e.g. asphalts, black shingles).	Hard to define 'Impervious-high albedo' with LCCS.
90 Barren Land						Vegetation is hardly observable but dominated by exposed soil, sand, gravel, and rock backgrounds.	
	91 Dry salt flats	Bare soil and/or unconsolidated material(s) with salt flats	B16	A5B13	6020	Dry salt flats occurring on the flat floored bottoms of interior desert basins.	
	92 Sandy areas	Loose and shifting sands	B16	A6	6006	Sandy areas are composed primarily of dunes accumulations of sand transported by wind.	
	93 Bare exposed rock	Gravels, stones and/or boulders/ bare rock(s)	B16	A3–A8/A3–A7	6002-2/6002-1	Gravel land and bare rocks.	
	94 Bare herbaceous croplands	Bare soil and/or other unconsolidated material(s)/// herbaceous croplands	B16///A11	A5///A3	6005///10025	Just harvested, fallow land and all other types of land not covered by vegetation such as lake bottoms in dry season.	

	95 Dry lake/river bottoms	Bare soil and/or other unconsolidated material(s)	B16///B28	A5/// A1–A5 A5/// A1–A4	6005///8001-5 6005///8001-4	Other types of land not covered by vegetation such as lake/river bottoms in dry season.
	96 Other barren lands	Bare soil and/or other unconsolidated material(s)	B16	A5	6005	All other types of land not covered by vegetation.
100 Snow and ice						Distributed in the polar areas and high mountains.
	101 Snow	Perennial snow/seasonal snow	B28	A2B1/A2B2	8006/8007	Lands under perennial or non-perennial snow over.
	102 Ice	Perennial ice/seasonal ice	B28	A3B1/A3B2	8009/2010	Lands under perennial or non-perennial ice over.
999 Cloud		N/A	N/A	N/A	N/A	

Note: LCCS, land-cover classification system (Di Gregorio 2005).

In this scheme, we try to avoid the use of the land use concept as much as possible. For example, only land covered by crops is included as cropland. Harvested agricultural land and grazed grassland with traces of cultivation are listed under barren land in consideration of their land-cover function. Similarly, there are areas that are seasonally varying. For example, lakes in arid areas can look like barren land during the dry season but like waterbodies during the wet season. Lakes in tropical and subtropical areas may exhibit totally different cover types ranging from bare land, vegetation, to water surfaces due to large fluctuation of water levels (e.g. Poyang Lake, the largest freshwater lake in China, Dronova, Wang, and Gong 2011). In training sample selection from the Landsat TM/ETM+ imagery, we followed a 'what you see is what you get' principle to prevent subjective inference of image information from apparent land use.

Based on these considerations, we did not include the urban class as it is a compound class reflecting land use. Wetland is a class that encompasses a large number of geomorphological sub-categories such as marine, estuarine, riverine, lacustrine, and palustrine wetlands (Cowardin et al. 1977). Temporally, they can be divided into permanent, seasonal, and intermittent. Spectrally, they vary among water, barren land, and vegetation. Vegetated marsh lands are probably the only spectrally unique wetland category that can be discerned from TM and ETM+ imagery. In addition, marshland is one of the most productive wetlands and is biologically significant for conservation reasons. At level 2, an inundated marsh-land with emergent vegetation is included as a wetland class. In addition, wet muddy bare land such as a wet lake bottom or a wet silt land at coastal areas that are spectrally unique is chosen as a second wetland class. At level 1, marshland is merged into grassland but wet muddy bare land is merged into bare land in consideration of their land-cover function. Forested wetlands and other wetlands are not specifically treated as individual classes and they will be extracted using special algorithms and additional data types such as surface hydrology, terrain, and SAR data in the future. Therefore, in this classification, we did not have a wetland class at level 1. Similarly, we did not have a specific land-cover class of tundra at level 1, as it is primarily composed of shrub and grass with a very short unfrozen growing season. The shrub tundra and grass tundra are defined as different classes at level 2 but separately merged into the shrub and grassland level 1 classes. In this fashion, barren land should include bare agricultural fields, dry season lake bottoms and seasonal river channels. This problem can be addressed by regrouping the second-level land-cover classes into level 1 classes. For example, harvested agricultural lands are merged into agricultural lands when needed. This problem can be better addressed by applying multitemporal data obtained from coarser resolution sensors such as MODIS or MERIS to produce the next generation land-cover map. A more complete wetland cover class, tundra, and land-use categories of agricultural land shall be separately extracted from time-series remotely sensed data in addition to other ancillary data such as terrain, hydrology, and climate data. Urban land will be extracted either with an object-based image segmentation and classification approach (Wang et al. 2010) or a cover-frequency approach (Gong and Howarth, 1992a, 1992b).

5. Training and test sample collection

Representative training samples are one of the most critical components in supervised classification. The quality as well as the quantity and distribution of these samples are all important. To collect a large volume of training data most efficiently, we used the following criteria to select training samples.

(1) Training samples must be homogeneous; land-cover mixtures and heterogeneous areas are avoided.
(2) All samples must be at least 8 pixels × 8 pixels in size to approximate a 250 m MODIS pixel size to support future classification of 250 m MODIS data.
(3) The land-cover category must be interpreted based on what can be derived from the TM image. Google Earth images and temporal data at the same location are treated as reference only.
(4) About 10–20 samples are required to be selected from each scene, and no more than three samples for each category (unless a scene is homogeneous, such as in the Sahara or tropical rainforest areas).
(5) Samples should be distributed in a scene as representative of the major classes present in the scene as possible.

Training samples were selected by traversing all 8929 available Landsat images. A total of 27 image analysts who have experience in remote-sensing image interpretation were selected to work on training sample collection in the initial round. Our training sample selection involved the following four steps.

(1) All 27 interpreters, including four test sample interpreters, were trained together for sample selection by the same group of experts, who are from or familiar with land-cover types of different areas of the world. Practice sessions were done over China. Several interpreters have field experiences in Canada, USA, Europe, and Australia.
(2) Initial interpretation: 23 of the 27 analysts performed the initial training sample selection according to the selection criteria.
(3) Initial interpretation results were passed to another interpreter for cross-checking.
(4) Cross-checked initial interpretation results were submitted to one of the four quality controllers for final checking.

The four quality controllers were selected from the 23 interpreters based on their distinguished interpretation performance (according to the quality and distribution of samples they had collected during the practice stage). They were requested to comment on the interpretation results and change the location of samples when the initial samples did not meet the sample selection criteria. When samples were not easy to interpret, quality controllers flagged them and entered a comment in a table of attributes (Table 4).

In the second round, training samples were refined by 10 high-quality image interpreters with additional information of time series vegetation index data from the 2010 annual MODIS EVI data product. The interpreters were evaluated for their strength and skill for different land-cover classes, and they were assigned to make refinement of the classes with which they were most familiar. The advantage of including the MODIS time series data was to help improve the separation between cultivated bare lands and natural barren lands, and distinguish sparsely vegetated land from more persistent barren land.

Table 4. Attributes for training sample collection.

ID	Img-name	Type code	Large sample	High resolution	Confidence	Cross-check	Quality control	Comment	Notes

The attribute table (Table 4) was designed to contain the following.

(1) ID: the ID for a sample in a scene.
(2) Image Name: the name of the Landsat image.
(3) Type Code: land-cover type according to the classification system.
(4) Large sample: empty if the sample is a large sample (indicating land cover is homogeneous, at least 500 m around a sample location), '0' otherwise.
(5) High resolution: empty if higher resolution (compared to 30 m in TM/ETM+) imagery is accessible on Google Earth at the sample location, '0' otherwise.
(6) Confidence: empty if the interpreter has confidence for this sample, '0' or '1' if he/she is 'not sure' (confusion at level 2, but sure for level 1) or 'highly uncertain' (confusion at level 1), respectively.
(7) Cross-check comment: Type Code when another interpreter does not agree with the initial interpreter.
(8) Quality controller comment: Type Code when the controller does not agree with the interpreter.
(9) Final comment: empty.
(10) Notes: other information relevant to the sample.

A customized set of software tools implemented in GM was provided to the interpreters. The software set allowed the interpreters to simultaneously open the Landsat imagery, location synchronized Google Earth imagery, and MODIS time-series vegetation index curve. Spectral curves and digital elevation data could be visualized as needed. Frequent meetings were held to discuss areas difficult to interpret. Before training on sample collection, some interpreters conducted field works in Canada, Russia, Western Europe, Middle Chile, and the tropical and temperate zones of Brazil. The sample collection began with China and then proceeded to Europe, where high resolution data are extensively available and reference maps can be checked for quality assurance. Regional experts from Russia, Europe, Africa, and the Tropics were brought in to help answer questions related to their areas of expertise. Several auxiliary data sets were provided to the interpreters for reference in sample selection/checking. They include the World Terrestrial Ecoregions Map (Olsen et al. 2001), Global Ecological Map of the World (FAO 2001), Atlas of World Physical Geography (Zheng, Mei, and Zhong 2009), and Atlas of China Physical Geography (Liu 2007). Additional Internet search efforts and discussions were made by individual interpreters when needed for solving uncertain issues.

In total, 91,433 training samples were collected. The distribution of these samples is shown in Figure 8. The proportions of different attributes (i.e. large sample, high resolution, confidence) of the samples are listed in Table 5. Although efforts were made to reduce uncertainties in training sample collection, approximately 4% of the training samples that were uncertain have been included in the classification.

In the first round, test samples were collected primarily by four image interpreters who did not participate in the training sample collection. Test samples were preset in a systematic unaligned manner. Their locations were fixed and could not be changed by the interpreters. First, the entire globe was partitioned by a hexagonal scheme (Icosahedral Snyder Equal Area Discrete Global Grids (ISEA DGGs)), which was generated from DGGRID software available online (http://webpages.sou.edu/~sahrk/dgg/dggrid/dggrid.html) such that the world's total land area was divided into approximately 7000 equal area hexagons (Figure 9). We initially randomly assigned 10 samples in each hexagon for China

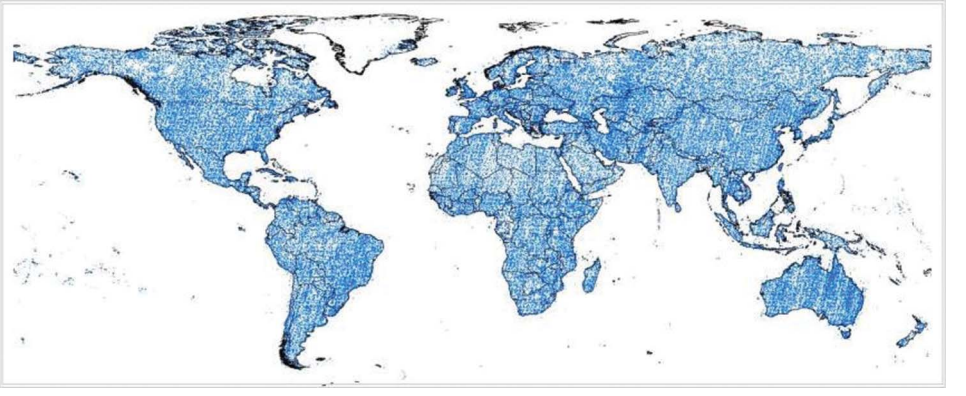

Figure 8. Training sample distribution (blue colour).

Table 5. Statistics of training sample attributes ($N = 91{,}433$).

Sample types and quality	Percent of total
Large sample – homogeneous area greater than 500 m × 500 m	77.04% (70,441/91,433)
High resolution images available in Google Earth	74.97% (68,551/91,433)
Confidence level – sure	95.75% (87,548/91,433)
Confidence level – not sure	4.12% (3770/91,433)
Confidence level – highly uncertain	0.13% (115/91,433)

and Europe. By evaluating the effect of the test sample density on resultant accuracy measures, we found that alteration of the number of samples per hexagon (between three and five) did not cause much change in the final accuracy assessment. For the whole world, we set five random samples for each hexagon. In the second round, we assigned three top quality image interpreters to make refinement of the test sample, with additional MODIS EVI time series data as reference.

According to the attribute requirement as specified in Table 6, we collected 38,664 test samples (Table 7 and Figure 10), 2034 of which were not used for accuracy assessment, leaving 36,630 valid test samples. The unused samples were discarded due to the fact that they did not meet minimal criteria (e.g. (1) 'very unsure' samples; (2) sample location is out of a scene (in background near the edge of an image); (3) samples located in the sea; and (4) samples located in shadows, under clouds, or on steep slopes).

6. Results

Figure 11 shows global land-cover maps derived from each classification algorithm. It can be seen that barren lands and forests are among the most abundant classes. Because there are significant temporal differences among the scenes, patch effects can be observed. Tables 8–11 list the confusion matrices corresponding to each classifier. These tables were calculated based on the 36,630 valid test samples. Among the four algorithms, the OAs at the global scale based on our test samples are 64.89%, 59.83%, 57.88%, and 53.88%, respectively, with the SVM, RF, J4.8, and MLC.

Among the classes, snow and ice are classified with the best accuracies (85.66% for the producer's accuracy and 95.61% for the user's accuracy). This is followed by waterbodies, barren lands, and forests. Impervious areas, croplands, grasslands, and shrublands are

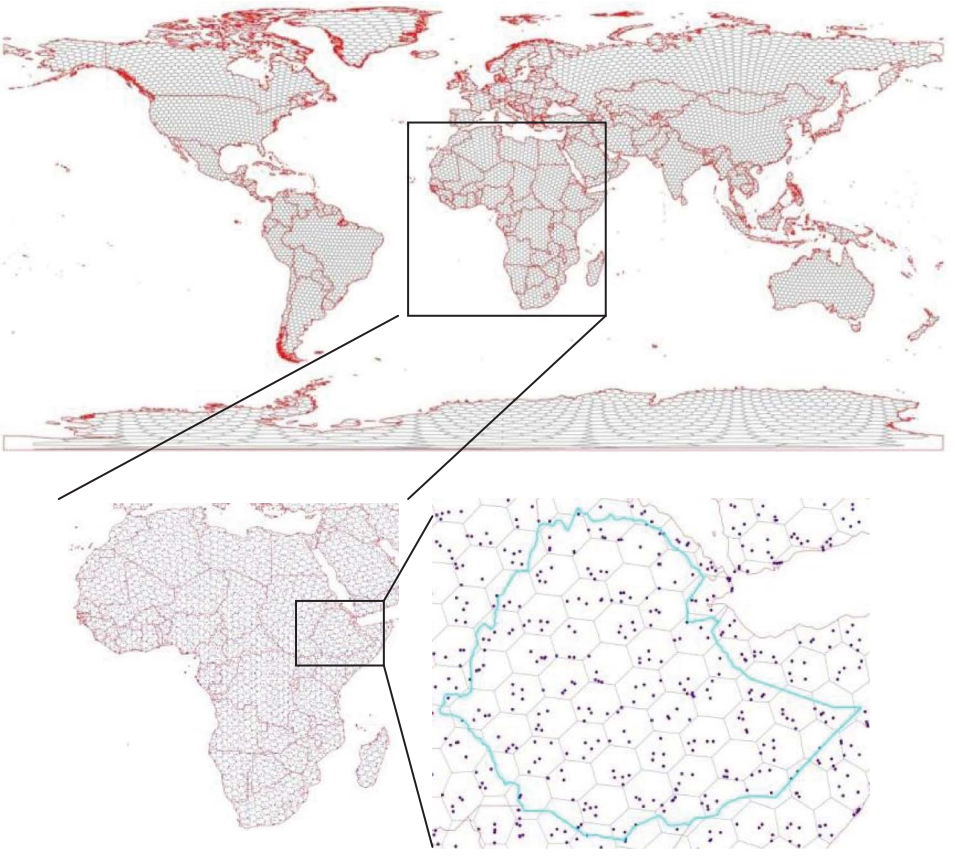

Figure 9. Test sample allocation design.

Table 6. Attributes for test sample collection.

ID	Img-name	Type code	Large sample	High resolution	Confidence	Pure	Cross-check	Quality control	Comment	Notes

Table 7. Summary of test samples ($N = 38{,}664$).

Sample types and quality	Percentage of total
Large sample – homogeneous area greater than 500 m × 500 m	37.82% (14,623/38,664)
High resolution images available in Google Earth	59.39% (22,962/38,664)
Confidence class – sure	80.80% (31,241/38,664)
Confidence class – not sure	12.42% (4798/38,664)
Confidence class – highly uncertain	6.78% (2625/38,664)
Pure pixel	62.43% (24,138/38,664)

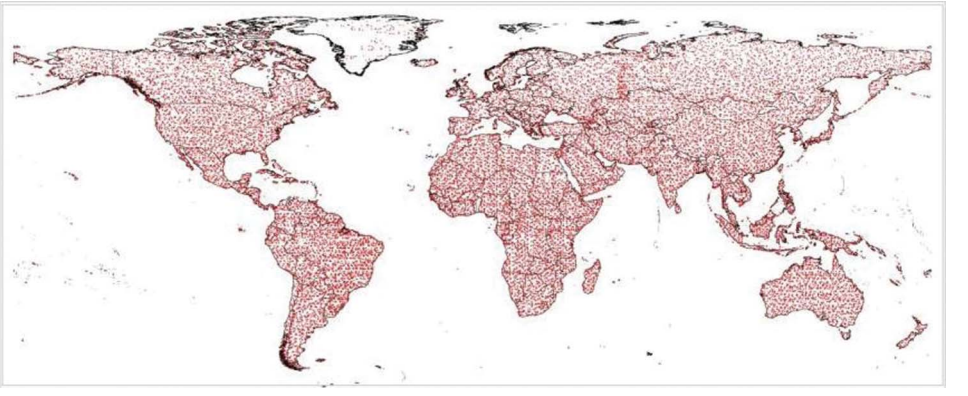

Figure 10. Distribution of test samples (red colour).

poorly classified. Some of the accuracies for impervious lands fall below 20%. The accuracies for croplands, grasslands, and shrublands are below 50%.

Although our focus is on the mapping of Level 1 classes that have been aggregated from the classification of Level 2 classes, it is relevant to present the confusion matrix for Level 2 classes obtained with the SVM as an example (Table 12). The OA for Level 2 classes is 52.76%. In the remainder of this article, we shall only discuss the mapping results for Level I classes.

The distribution of wrongly classified sample locations (Figure 12) can be seen clearly. Errors are distributed along transitional zones such as the South Sahel from dry to humid climates, the boreal ecosystem ecotones of forests, shrubs, grasslands and wetlands, and some of the mountain ranges such as the Rocky Mountains, and the east edge of the Andes. In addition, Kazakhstan, southeast Europe, and India are particularly problematic.

At the continental level, all continents are classified between 50% and 70% OA with Oceania at the low end and Africa at the high end (Table 13).

If we single out big, pure samples that have high resolution Google Earth imagery for verification, the OA from the SVM increases to 71.5% globally (Table 14). With these samples, the certainty of land-cover interpretation is high. This group of samples can be used to assess other global land-cover products such as those produced with MODIS and MERIS. Table 13 represents the best accuracy we observed in the 30 m land-cover products.

The classification accuracies can also be analysed at the national level. Table 15 lists the OAs of the top 50 countries that are ranked by area. The total area of these countries accounts for 86% of the global land territory. Among the top 10 largest countries, the classification accuracy of only Kazakhstan falls below 50% (Table 15). This is largely caused by confusion between croplands and pasture, which when looked at from a land-use perspective should be considered to be agricultural land and when looked at from a land-cover perspective should be considered to be grassland. The worst accuracies are found in Africa. The classification accuracy of South Sudan falls below 40%. All but two countries in the top 50 falling below 50% are found in Africa including Angola, Ethiopia, Tanzania, Mozambique, Zambia, South Sudan, Central Africa, and Kenya. The other two countries are Kazakhstan and Thailand. From Figure 13, it can be seen that the arid areas are best classified but the southern half of Africa has the lowest classification accuracy. Out of the

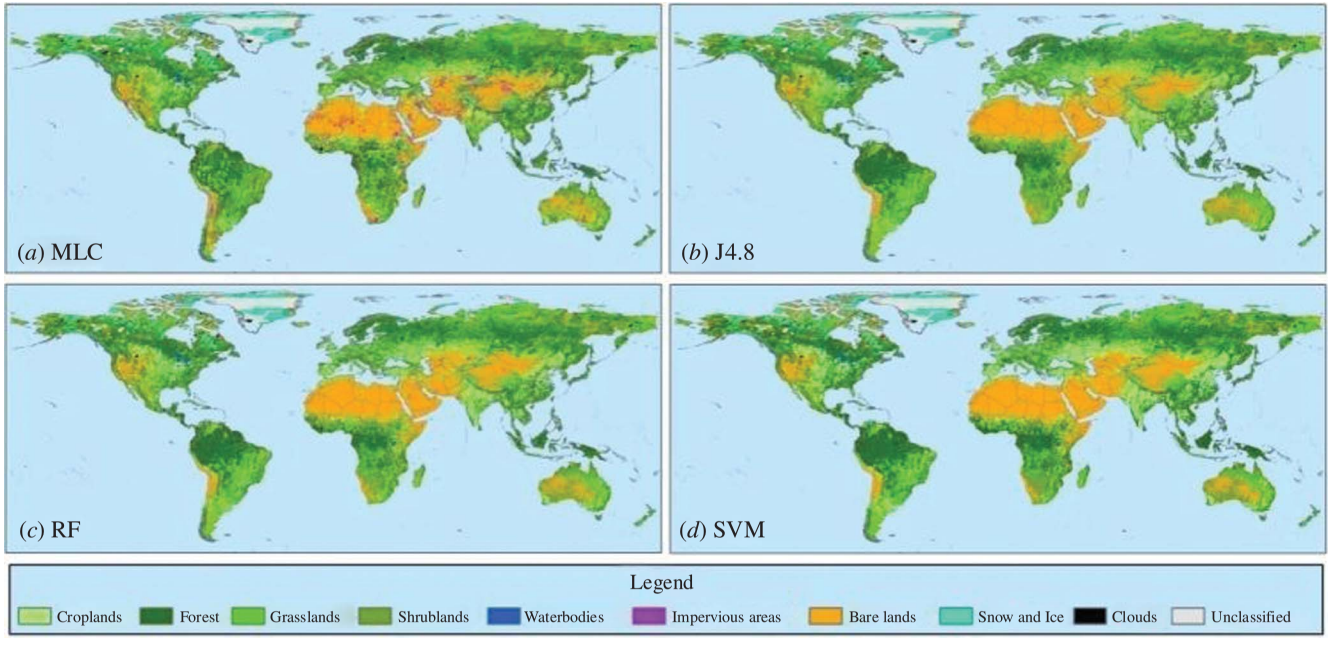

Figure 11. A synoptic view of the global land-cover products derived with MLC (*a*), J4.8 (*b*), RF (*c*), and SVM (*d*).

Table 8. Confusion tables for the global land-cover map product derived with SVM.

SVM	Croplands	Forests	Grasslands	Shrublands	Waterbodies	Impervious areas	Bare lands	Snow and ice	Clouds	Total number	UA (%)
Croplands	**1091**	667	453	78	10	33	62	1	15	2410	45.27
Forests	459	**8874**	843	684	49	35	38	1	42	11,025	80.49
Grasslands	445	862	**2062**	966	20	28	268	5	17	4673	44.13
Shrublands	152	567	473	**1571**	1	9	391	0	0	3164	49.65
Waterbodies	22	121	49	23	**1272**	4	61	19	8	1579	80.56
Impervious areas	5	4	4	5	5	**28**	28	0	12	91	30.77
Bare lands	599	399	1981	1287	58	125	**7653**	41	58	12,201	62.72
Snow and ice	0	6	5	2	9	0	4	**675**	5	706	95.61
Clouds	8	108	42	13	9	4	7	46	**544**	781	69.65
Total number	2781	11,608	5912	4629	1433	266	8512	788	701	**36,630**	
PA (%)	39.23	76.45	34.88	33.94	88.76	10.53	89.91	85.66	77.60		64.89

Note: Numbers of correctly classified testing samples are in bold.

Table 9. Confusion tables for the global land-cover map product derived with RF classified.

RF	Croplands	Forests	Grasslands	Shrublands	Waterbodies	Impervious areas	Bare lands	Snow and ice	Clouds	Total number	UA (%)
Croplands	**1059**	928	529	173	19	27	107	0	9	2851	37.14
Forests	378	**7762**	693	654	53	44	74	5	58	9721	79.85
Grasslands	527	1138	**2010**	989	51	33	382	6	13	5149	39.04
Shrublands	170	960	630	**1361**	3	8	436	0	1	3569	38.13
Waterbodies	47	210	81	46	**1215**	4	86	20	9	1718	70.72
Impervious areas	27	36	33	32	9	**42**	139	1	30	349	12.03
Bare lands	561	456	1889	1355	70	104	**7273**	40	54	11,802	61.63
Snow and ice	0	7	7	2	9	0	6	**671**	6	708	94.77
Clouds	12	111	40	17	4	4	9	45	521	763	68.28
Total number	2781	11,608	5912	4629	1433	266	8512	788	701	**36,630**	
PA (%)	38.08	66.87	34.00	29.40	84.79	15.79	85.44	85.15	74.32		59.83

Note: Numbers of correctly classified testing samples are in bold.

Table 10. Confusion tables for the global land-cover map product derived with J4.8 classifier.

J48	Croplands	Forests	Grasslands	Shrublands	Waterbodies	Impervious areas	Bare lands	Snow and ice	Clouds	Total number	UA (%)
Croplands	**1032**	979	536	208	27	31	160	0	13	2986	34.56
Forests	411	**7567**	764	646	59	39	136	7	58	9687	78.11
Grasslands	522	1181	**1912**	1018	52	37	447	6	14	5189	36.85
Shrublands	192	962	637	**1281**	6	8	461	2	2	3551	36.07
Waterbodies	47	242	103	64	**1192**	7	94	20	5	1774	67.19
Impervious areas	34	51	66	44	14	**43**	204	3	31	490	8.78
Bare lands	532	505	1846	1350	66	98	**6993**	36	58	11,484	60.89
Snow and ice	0	8	7	4	9	0	5	**671**	11	715	93.85
Clouds	11	113	41	14	8	3	12	43	**509**	754	67.51
Total number	2781	11,608	5912	4629	1433	266	8512	788	701	**36,630**	
PA (%)	37.11	65.19	32.34	27.67	83.18	16.17	82.15	85.15	72.61		57.88

Note: Numbers of correctly classified testing samples are in bold.

Table 11. Confusion tables for the global land-cover map product derived with MLC.

MLC	Croplands	Forests	Grasslands	Shrublands	Waterbodies	Impervious areas	Bare lands	Snow and ice	Clouds	Total number	UA (%)
Croplands	**697**	844	425	238	21	16	84	0	5	2330	29.91
Forests	479	**6579**	611	642	60	27	53	0	21	8472	77.66
Grasslands	692	1404	**1826**	795	51	44	347	2	12	5173	35.30
Shrublands	335	1827	1148	**1319**	6	7	408	0	2	5052	26.11
Waterbodies	32	210	73	36	**1162**	4	81	15	4	1617	71.86
Impervious areas	82	166	180	190	28	**89**	619	6	71	1431	6.22
Bare lands	442	366	1590	1376	67	76	**6881**	43	51	10,892	63.17
Snow and ice	3	14	7	5	17	0	6	**654**	5	711	91.98
Clouds	19	198	52	28	21	3	33	68	**530**	952	55.67
Total number	2781	11,608	5912	4629	1433	266	8512	788	701	**36,630**	
PA (%)	25.06	56.68	30.89	28.49	81.09	33.46	80.84	82.99	75.61		53.88

Note: Numbers of correctly classified testing samples are in bold.

Table 12. Confusion table for the global land-cover map product derived with SVM for Level II classes.

	999	11	12	13	21	22	23	24	31	32	40	51	52	61	62	63	64	71	72	81	82	91	92	93	94	95	96	101	102	Sum	UA (%)
999	**544**	0	0	8	76	19	11	2	2	15	4	1	1	3	1	2	3	9	24	3	1	1	1	3	1	0	0	41	5	781	69.65
11	0	**21**	0	5	17	1	1	1	0	0	0	3	0	1	1	2	2	0	0	0	0	1	1	1	2	0	0	0	0	60	35.00
12	0	0	**0**	0	0	2	0	0	0	0	0	0	0	0	0	0	0	1	0	0	0	0	0	0	0	0	0	1	0	4	0.00
13	14	14	1	**1050**	474	67	68	36	114	315	77	21	0	3	1	0	0	0	0	12	21	1	1	3	52	0	0	0	0	2345	44.78
21	42	3	0	415	**5259**	249	303	85	119	282	467	58	3	3	2	2	24	0	0	14	19	0	2	4	16	0	0	0	0	7371	71.35
22	0	0	0	31	194	**2206**	327	6	12	234	125	38	0	16	0	0	2	87	86	0	2	0	0	8	4	0	1	1	0	3380	65.27
23	0	0	0	10	136	49	**47**	1	0	14	4	0	0	0	0	0	0	0	0	0	0	0	0	0	0	0	0	0	0	261	18.01
24	0	0	0	0	10	0	0	**0**	0	0	1	0	0	0	0	0	0	0	0	0	0	0	0	0	0	0	0	0	0	11	0.00
31	0	0	0	9	5	0	0	0	**6**	4	1	0	0	0	0	0	0	0	0	1	0	0	0	0	0	0	0	0	0	26	23.08
32	16	0	0	430	453	224	100	12	114	**1128**	636	38	3	1	0	0	4	72	180	13	14	4	3	132	81	3	29	2	0	3692	30.55
40	0	2	0	150	445	99	16	7	32	392	**1546**	24	0	1	0	0	0	6	9	2	7	1	39	205	136	1	9	0	0	3129	49.41
51	1	0	0	6	26	15	1	0	0	8	11	**35**	0	8	0	4	0	9	13	0	0	1	0	2	0	1	0	0	0	141	24.82
52	0	0	0	1	0	0	0	0	0	0	2	0	**0**	2	0	0	0	0	0	0	0	2	0	1	1	1	0	2	0	12	0.00
61	1	0	0	4	37	20	6	0	1	12	9	10	4	**653**	3	48	196	3	6	0	1	1	4	17	0	1	0	11	3	1051	62.13
62	0	2	0	4	9	3	0	0	0	0	1	2	0	41	**21**	17	38	0	0	1	1	0	0	0	3	0	0	0	0	143	14.69
63	6	6	0	6	36	7	1	0	0	2	6	8	8	44	6	**65**	37	3	4	0	1	0	2	5	8	1	0	2	3	267	24.34
64	1	0	0	0	2	0	0	0	0	1	1	1	1	8	1	4	**90**	0	2	0	0	0	2	4	0	0	0	0	0	118	76.27
71	0	0	0	0	0	0	0	0	0	4	0	4	0	0	0	0	0	**19**	8	0	0	0	0	0	0	0	0	0	0	35	54.29
72	0	0	0	0	2	18	6	0	0	28	3	10	0	1	0	0	2	234	**498**	0	0	0	0	9	0	0	0	3	0	814	61.18
81	7	0	0	1	0	0	0	0	1	0	1	0	0	0	0	0	0	0	0	**4**	1	2	2	6	3	0	0	0	0	28	14.29
82	5	0	0	4	3	0	0	1	0	2	3	1	5	1	1	0	3	1	0	10	**13**	0	1	3	5	0	1	0	0	63	20.63
91	3	0	0	0	0	0	0	1	0	3	6	1	1	0	0	1	0	0	0	1	0	**16**	4	9	0	3	0	5	0	54	29.63
92	5	0	0	0	1	1	0	0	1	16	105	0	2	0	0	0	1	0	5	4	0	5	**1530**	852	27	8	2	4	1	2570	59.53
93	35	0	0	26	20	102	17	0	24	699	596	27	6	14	1	9	16	115	419	19	19	26	439	**2704**	208	26	26	23	0	5616	48.15
94	10	8	3	559	165	43	18	29	98	637	432	20	4	1	3	3	1	8	19	33	47	3	40	315	**1305**	9	24	0	1	3838	34.00
95	5	0	0	0	1	0	0	0	0	6	2	2	0	2	0	0	2	0	0	1	0	14	3	19	0	**4**	0	5	0	66	6.06
96	0	0	0	2	1	0	0	0	0	3	21	1	0	0	0	1	1	0	0	1	0	0	0	7	5	1	**1**	0	0	45	2.22
101	4	0	0	0	0	5	1	0	0	4	1	0	0	0	0	0	0	1	0	0	0	0	0	4	0	0	0	**478**	12	510	93.73
102	1	0	0	0	0	0	0	0	0	1	0	0	0	8	0	1	0	0	0	0	0	0	0	0	0	0	0	104	**81**	196	41.33
Sum	700	56	4	2721	7372	3130	923	181	524	3810	4061	305	38	811	41	159	422	568	1273	119	147	78	2074	4313	1857	59	93	682	106	36,627	
PA (%)	77.71	37.50	0.00	38.59	71.34	70.48	5.09	0.00	1.15	29.61	38.07	11.48	0.00	80.52	51.22	40.88	21.33	3.35	39.12	3.36	8.84	20.51	73.77	62.69	70.27	6.78	1.08	70.09	76.42		52.76

Note: Numbers of correctly classified testing samples are in bold.

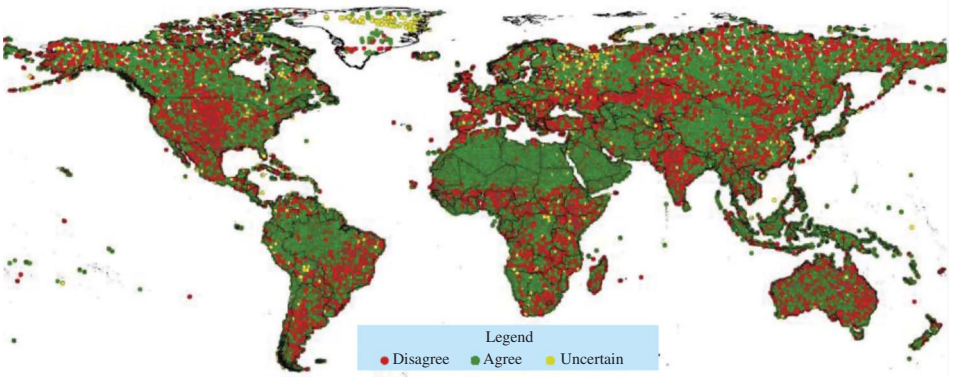

Figure 12. Test sample distributions based on the SVM classification algorithm. Red, wrongly classified; green, correctly classified; yellow, unused uncertain samples.

Table 13. A summary of OAs by continents in four land-cover data products based on self-collected testing samples that are labelled N and 'certainty' $= 1$ ($N = 36{,}630$).

	SVM (%)	RF (%)	MLC (%)	J4.8 (%)
Africa	69.54	64.32	57.28	62.28
Asia	67.49	62.21	55.73	59.89
Europe	62.03	56.40	49.84	53.37
North America	57.90	54.74	50.63	53.52
Oceania	58.87	52.92	51.78	50.88
South America	66.65	60.22	52.32	58.95
Global	64.89	59.83	53.88	57.88

Table 14. A summary of OAs by continents in four land-cover data products.

	SVM (%)	RF (%)	MLC (%)	J4.8 (%)
Africa	69.75	64.34	57.57	62.81
Asia	77.65	72.42	65.60	69.04
Europe	64.41	57.63	53.51	55.21
North America	65.44	61.78	56.44	61.33
Oceania	68.55	60.48	61.29	58.06
South America	69.27	63.00	57.73	60.45
Global	71.54	66.08	60.09	63.84

Note: Sample excluding N and large samples AND having high resolution data AND samples are pure AND pure samples using self-collected testing samples ($N = 8629$).

50 countries, the SVM achieved the greatest OCA for 46 of them. The RF classifier was the best performer in two countries, and J4.8 was the best performer for two other countries (including ties).

Based on the SVM land-cover map, we ranked countries in terms of abundance for each land-cover class. Among various classes, the rankings for forests, barren lands, waterbodies, snow and ice, and croplands have higher levels of certainty due to their relatively high level of test accuracies (Table 16). China has the greatest cropland area and bare land area; Russia has the greatest forest area; Canada has the greatest water surface area and area of snow and ice.

Table 15. Overall classification accuracies of the top 50 countries with greatest land territories.

Country	Area rank	J4.8 (%)	MLC (%)	RF (%)	SVM (%)	Average (%)
Russia	1	54.76	52.78	57.78	**62.93**	57.06
Canada	2	58.90	54.71	60.69	**63.52**	59.46
United States of America	3	49.15	48.12	50.26	**52.33**	49.96
China	4	56.95	55.94	60.61	**66.23**	59.93
Brazil	5	58.57	49.94	59.45	**65.48**	58.36
Australia	6	47.61	49.45	49.88	**55.90**	50.71
India	7	49.49	44.95	52.40	**56.06**	50.73
Argentina	8	46.50	46.78	47.48	**55.60**	49.09
Kazakhstan	9	**41.91**	39.88	40.32	38.87	40.25
Democratic Republic of the Congo	10	62.35	47.21	63.55	**69.12**	60.56
Algeria	11	93.02	86.82	94.57	**96.90**	92.83
Mexico	12	41.37	36.92	40.51	**50.26**	42.27
Saudi Arabia	13	91.65	88.52	93.74	**97.08**	92.75
Indonesia	14	65.48	52.51	68.41	**78.24**	66.16
Sudan	15	76.80	71.73	77.87	**80.80**	76.80
Libya	16	90.63	93.23	93.75	**97.66**	93.82
Iran	17	75.58	67.53	76.88	**83.38**	75.84
Mongolia	18	**57.19**	50.34	55.48	53.08	54.02
Peru	19	75.78	58.20	75.39	**78.13**	71.88
Chad	20	71.48	66.55	73.24	**78.87**	72.54
Mali	21	84.08	78.89	85.12	**90.66**	84.69
Angola	22	37.32	35.21	34.86	**40.85**	37.06
South Africa	23	37.09	39.74	37.75	**43.05**	39.40
Niger	24	85.92	84.48	87.73	**91.70**	87.45
Colombia	25	61.60	54.85	63.71	**70.89**	62.76
Ethiopia	26	43.97	41.25	43.58	**48.25**	44.26
Bolivia	27	68.24	60.09	70.39	**74.68**	68.35
Mauritania	28	88.40	83.20	89.60	**91.60**	88.20
Egypt	29	91.59	83.64	94.86	**95.79**	91.47
United Republic of Tanzania	30	36.45	39.72	39.25	**46.26**	40.42
Venezuela	31	59.90	56.44	64.36	**72.28**	63.24
Nigeria	32	42.99	39.72	44.86	**51.87**	44.86
Pakistan	33	62.79	53.95	66.05	**69.30**	63.02
Namibia	34	61.19	57.99	72.15	**79.00**	67.58
Mozambique	35	34.31	30.88	34.80	**46.08**	36.52
Turkey	36	44.80	47.96	47.51	**50.23**	47.62
Zambia	37	40.51	50.00	45.57	**49.37**	46.36
Chile	38	69.63	67.54	71.20	**74.35**	70.68
Myanmar	39	59.12	50.83	61.88	**75.69**	61.88
Afghanistan	40	70.50	64.03	71.94	**75.54**	70.50
France	41	58.05	51.69	56.55	**59.55**	56.46
South Sudan	42	26.40	19.20	**34.40**	29.60	27.40
Central African Republic	43	50.69	35.42	**55.56**	45.14	46.70
Ukraine	44	46.90	44.83	53.79	**62.76**	52.07
Madagascar	45	38.94	32.21	39.42	**52.40**	40.75
Kenya	46	37.09	31.13	36.42	**41.72**	36.59
Morocco	47	76.88	67.05	73.99	**80.35**	74.57
Botswana	48	60.71	35.71	67.86	**75.00**	59.82
Thailand	49	42.55	31.91	41.13	**49.65**	41.31
Spain	50	43.48	45.34	43.48	**51.55**	45.96

Note: The best accuracy is in bold.

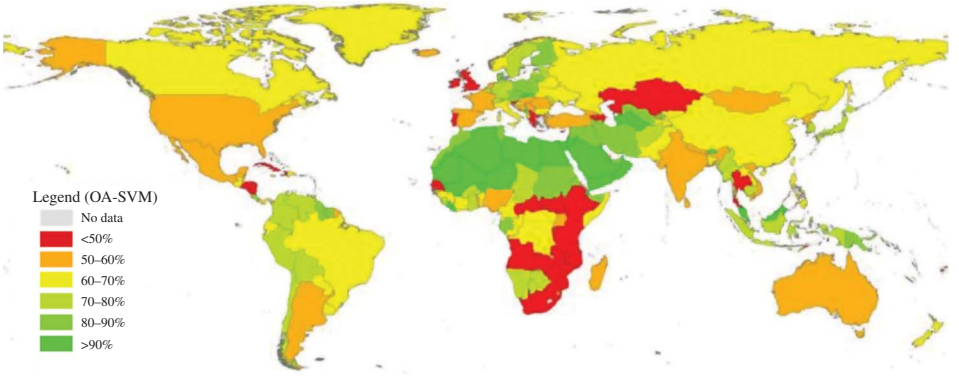

Figure 13. Overall accuracy (SVM) distribution for all countries in the world.

Table 16. The top 10 countries with the greatest abundance of some major cover classes obtained with the SVM.

Rank	Croplands	Area (km^2)	Forest	Area (km^2)	Waterbodies	Area (km^2)
1	China	2.79E+06	Russia	6.61E+06	Canada	8.10E+05
2	United States of America	2.42E+06	Brazil	4.70E+06	Russia	5.28E+05
3	India	1.98E+06	Canada	3.42E+06	China	3.41E+05
4	Russia	1.92E+06	United States of America	3.14E+06	United States of America	3.38E+05
5	Brazil	1.43E+06	China	1.71E+06	Brazil	1.62E+05
6	Kazakhstan	9.33E+05	Zaire	1.62E+06	Australia	7.22E+04
7	Argentina	7.69E+05	Indonesia	1.34E+06	Indonesia	6.94E+04
8	Canada	6.71E+05	India	8.02E+05	Chile	6.12E+04
9	Australia	6.27E+05	Peru	7.31E+05	India	6.04E+04
10	Mexico	5.55E+05	Colombia	6.68E+05	Tanzania	6.01E+04

Rank	Bare lands	Area (km^2)	Snow and ice	Area (km^2)
1	China	3.14E+06	Canada	7.73E+05
2	Algeria	2.16E+06	China	2.51E+05
3	Saudi Arabia	1.91E+06	Russia	2.37E+05
4	Australia	1.61E+06	United States of America	1.89E+05
5	Sudan	1.59E+06	India	4.98E+04
6	United States of America	1.58E+06	Pakistan	3.71E+04
7	Libya	1.56E+06	Chile	3.64E+04
8	Russia	1.40E+06	Kazakhstan	3.36E+04
9	Kazakhstan	1.37E+06	Afghanistan	1.55E+04
10	Canada	1.33E+06	Argentina	1.03E+04

Based on our test sample and the SVM results, we estimated the proportions of major land-cover classes (Table 17). Since the test samples were carefully interpreted, the proportion obtained from test samples should be closer to the reality. The percentage (adj.) is the area coverage calculated for all the land areas including Antarctica and Greenland. The small percentage of test samples identified as clouds was excluded in the percentage

Table 17. Global proportions of land-cover categories based on the SVM-based classification results and calculated from validation samples (proportion adjusted to include Antarctica and Greenland as Snow and ice, and clouds areas were excluded and normalized).

	SVM			Validation samples (Total 38,664)	
Category	Area	Percentage	Percentage (adj.)	Percentage	Percentage (adj.)
Croplands	7.77E+06	6.07	5.47	7.59	6.90
Crop + Bare land crop. field	2.23E+07	17.44	15.71	12.66	11.51
Forest	3.73E+07	29.19	26.29	31.19	28.35
Grasslands	1.50E+07	11.72	10.56	14.71	13.37
Shrublands	1.24E+07	9.72	8.76	12.64	11.49
Waterbodies	3.95E+06	3.09	2.78	3.91	3.56
Impervious areas	2.41E+05	0.19	0.17	0.73	0.66
Bare lands	3.28E+07	25.62	23.08	18.17	16.51
Snow and ice	1.96E+06	1.53	12.60	2.15	12.81
Clouds	1.85E+06	1.45	–	1.91	–

(adj.) with a normalization process that takes the ratio between the total area of each land cover (except the cloud) and the difference between the total land area and the cloud area. At the global level, only the percentage (adj.) is a meaningful coverage indicator of various land-cover types.

In an attempt to use the SVM land-cover map product in Jiangxi Province, China, which is a mountainous area with 167,000 km^2, an independent accuracy assessment was done by ourselves with 350 randomly selected test samples collected by a third-party group of researchers familiar with that region. The OA achieved was 65.1%. This is close to the OA of 66.2% for China.

Figure 14 compares FAO national surveys conducted in 2009 for arable lands of the top 50 countries the with the areas mapped with the SVM classifier (Figure 14(*a*)) or with those estimated from the test samples (Figure 14(*b*)). The area estimated from test samples is done by taking the product of the total area of a country and the proportion of samples among the total test samples for a country. The FAO results were derived from country-supplied statistics. FAO arable lands include land under temporary crops (double-cropped

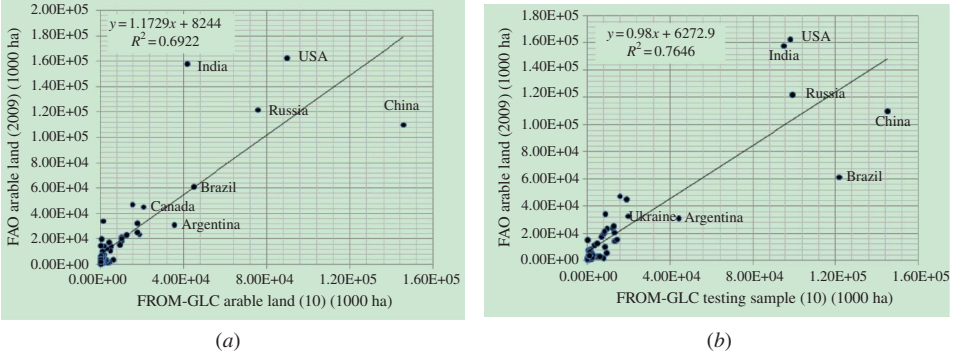

(*a*) (*b*)

Figure 14. Comparison of arable lands between FAO survey and FROM-GLC.

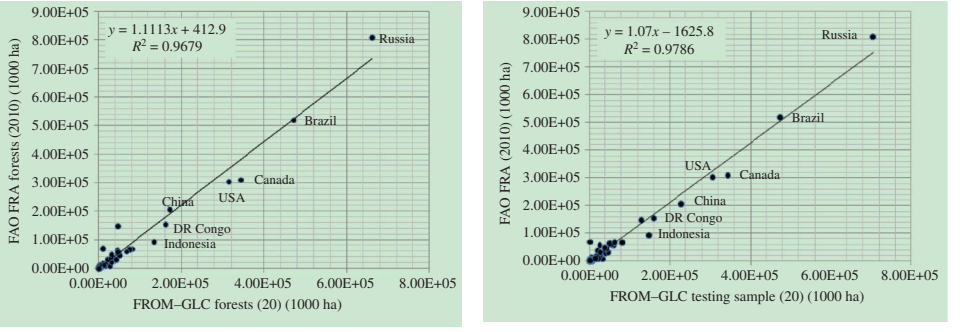

(*a*) (*b*)

Figure 15. Comparison of forests areas between FAO survey and FROM-GLC.

areas are counted once), temporary meadows for mowing or for pasture, land under market or kitchen gardens, and land temporarily fallow. Neither land abandoned as a result of shifting cultivation nor permanent crops such as orchards and vineyards are included. This closely matches our cropland category except that we treated temporary fallow land under barren land and mowed meadows and cultivated pastures under grassland in consideration of their land-cover types as observed from the satellite data. From Figure 15(*a*), it can be seen that in general the SVM classification results are about 17% lower than the FAO survey and the goodness of fit has an R^2 of 0.69. The greatest discrepancy is found for China, India, and the USA. In the case of China, the FAO data give only 1.1 million km^2, whereas the SVM map results give 1.55 million km^2. For India, the FAO data give 1.58 million km^2, whereas the SVM results only report 400,000 km^2. The cropland for the USA is also substantially undermapped by the SVM. The FAO ranks the USA, India, Russia, China, and Brazil as the top five countries with the greatest agricultural area while the rank order by the SVM is China, the USA, Russia, Brazil, and India. Comparing the FAO data with the cropland area estimated from the test samples, the slope of regression is close to 1 indicating a better general agreement at the global scale (Figure 15(*b*)). The R^2 also increased to 0.75. However, a great discrepancy still exists when the results are compared country by country. The order of the top five agricultural countries is China, Brazil, Russia, the USA, and India. Reasons for the differences are out of the scope of this study.

Figure 15 compares FAO national surveys conducted in 2009 with forest areas mapped with the SVM classifier or those estimated from the test samples for forest land. FAO defined forest area as land under natural or planted stands of trees of at least 5 m height *in situ*, whether productive or not, and excludes tree stands in agricultural production systems (for example, in fruit plantations and agroforestry systems) and trees in urban parks and gardens. Our mapping results also excluded the agroforestry systems such as orchards and vineyards but did not have an explicit requirement of 5 m height. Our definition of forest is based on whether a clear stem is observable to distinguish between shrubs and forest. The goodness of fit is much better here, both greater than 0.96. Despite not having a minimum height limit, both the SVM classification results and the estimated forest area from the test samples are 11–14% lower than the FAO survey results.

7. Discussions and perspectives

High-quality land-cover classification is determined by a number of factors (Gong and Howarth 1990; Cihlar 2000; Foody 2002). They include classification scheme, quality of

input variables for mapping, training samples, and classifiers used. Classification scheme is often determined by the purpose of mapping and class separability of input variables. Input variables, also referred to as features, are often solely composed of various bands of images or their combinations and less often ancillary data layers such as elevation and climate data. The common practice in global land-cover mapping is the use of multitemporal images that are acquired in a specific year. These are difficult to obtain for medium resolution data. Since Landsat data have only recently become freely accessible, we only managed to collect a single coverage from images obtained in a multiannual span. While this is an obvious shortcoming of this first attempt, its value is also obvious because compared to the 30–40% classification errors the magnitude of land-cover change in different years can be negligible. Despite this, more timely and consistent multitemporal data should be used to improve the classification when they become available in the future as demonstrated in regional studies (Potapov et al. 2012); or a combination of less frequently available medium resolution data with more frequently available coarser resolution data should be implemented. Although we have used tens of thousands of training samples and compared four different classification algorithms, efforts reported here can only be considered as an initial attempt for global land-cover mapping using medium resolution satellite imagery. We have only seen the tip of the iceberg and a large amount of evaluation experiments need to be done in the future.

The level of image processing over the entire world could be standardized in the future. For example, due to inconsistent formats among the 519 scenes collected from the Chinese Satellite Ground Station, we did not carry out radiometric and topographic correction over China. Additional efforts will be made to collect data that have been more professionally processed for global land-cover mapping.

While the training and test databases may seem large, we consider what has been tested in this study to be minimal. Reducing the number of validation points by half in China and Europe, we experimented and found little change in accuracy values. It seems that at the global scale, the total number of test samples may be adequate. However, the global land-cover classification can definitely benefit from a greater number of, and more importantly representative, training samples. In our experiments, no matter how we augment the samples, either by taking local neighbourhood pixels around the selected training sample location or by including a larger number of training sites in neighbourhood scenes, the resulting accuracies seem to increase for most classes except impervious surfaces. With this category, a 3×3 window used surrounding the training sample pixel location produced better results than bigger window sizes.

There are a number of possibilities in experimentally determining the most effective way to increase the training data-set size. Among the alternatives are the following.

(1) There are over 38,000 test samples. At least half of them could be used in training without significantly impacting the accuracy assessment. We did some experiments with the inclusion of one-third of the test samples randomly selected for training and obtained an average increase of 8% in the OA. Because test samples were prefixed by location and interpretation had to be done regardless of whether they were pure pixels or mixed, the inclusion of a portion of the test samples increased the representativeness of the training data that led to improved accuracy. Another reason could be because those test samples were collected by another small group of image interpreters who created an inevitable inconsistency in interpretation compared to the training sample interpreters. This mixing of training and test samples reduced the discrepancy between the training and test samples.

(2) At higher latitudes, Landsat images have a large amount of overlap. Training samples in the overlapped portions could be pooled together to evaluate the potential for accuracy improvement by increasing the number of training samples.
(3) The overlapped portions could also be used to evaluate a chain classification strategy (Knorn et al. 2009), other signature expansions and adaptive learning techniques (Olthof, Buston, and Fraser 2005; Tuia, Pasoli, and Emery 2011), or efficacy of efficient image clustering to aid classification (Chen and Gong, submitted).
(4) Ongoing training sample collection and refinement. Although we have made efforts to do two rounds of sample refinement, there are still some samples that are either uncertain or lacking the evidential support by higher resolution data. Innovative technologies for simultaneous collaborative sample identification by multiple interpreters are needed to refine the existing training samples.
(5) Crowd sourcing and collaborative learning system development. Field work and crowd-sourcing sample collection (e.g. http://www.geo-wiki.org) to augment the training data should be used when possible. Lastly, training and test sample collection should be strengthened through international collaboration as has been done by Taseichi et al. (2011).

One of the unique contributions of this research is the collection of a large number of test samples. Because of the systematic unaligned nature of the test samples and scale range (30–500 m), they could serve as a valuable resource for validating other classification efforts in parts of the world other than Greenland and Antarctica.

Gathering training and test samples from the image to be classified has a large amount of uncertainty (Powell et al. 2004). The use of ancillary data can help alleviate this problem. The GM and GA software packages were developed to facilitate the incorporation of massive amounts of ancillary image data to global mapping projects. Spatialization of other published studies on land-cover mapping could also aid in the synthesis of the global knowledge base.

Similar to other global land-cover mapping efforts, this research also adopted a per-pixel classification approach. Image segmentation was run on all scenes used in this study with a fast watershed segmentation algorithm (Wang et al. 2010). Initial experiments were done to mode-filter classification results in each segment as a postprocessing procedure. While this post-process filtering method has improved the OA by approximately 3% for the classification results derived by the RF classifier, we have not achieved improvement in the SVM results. In depth analysis of the reasons is in progress. The next step would be experimenting with object-based image classification approaches.

Figure 16 presents some selected and wrongly classified test samples from various areas. Ten sample images were selected from the worst-classified scenes in the world. From a first glimpse of the distribution, the red areas seem to not escape the spell of Jung et al. (2006) and Herold et al. (2008) that heterogeneous land-cover areas would be poorly classified. Except desert and tropical forest areas, all other land-cover types are poorly classified. Indeed, as can be seen from the samples, typical confusions happened among non-tropical natural vegetation classes: forests, shrubs, and grasslands. Additionally, confusions occurred among low-density vegetation areas and bare lands. It seems that most of the mistakes are constrained to the vicinity of our sample locations. We regard them as reasonable due to the lack of spectral separability and the constraint of per-pixel classification. However, sample image #3 in Central Asia where large tracts of natural grasslands were classified as bare croplands is quite unacceptable. The reason could be partly due to spectral confusion and partly due to the inadequate training samples used. This area along with

ID	Landsat Bands 4/3/2 composites	Classified results (SVM)	Classified results (RF)
1		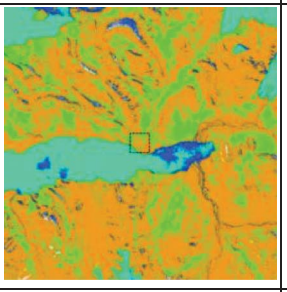	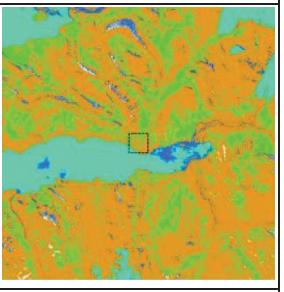
	(1) p051r003_7dt19990708 (2) Canada (3) Lat/Lon: 79.245166°/–90.722042° (4) Ecoregion: high arctic tundra Test sample: herbaceous tundra classified as bare field. Due to lack of high resolution image, uncertainty exists in judging the density of vegetation coverage. This is a reasonable confusion.	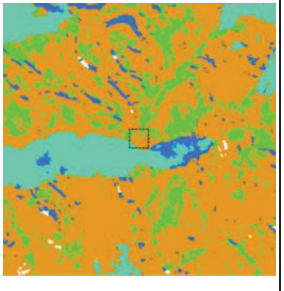	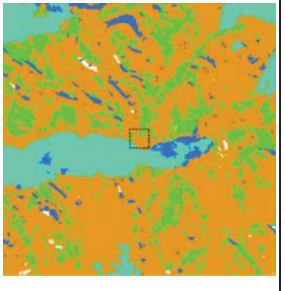
		72 classified as 93	72 classified as 93
2		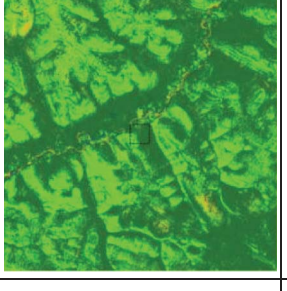	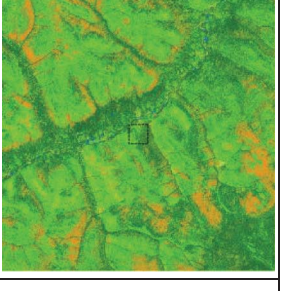
	(1) l5131013_01320100715 (2) Russia (3) Lat/Lon: 67.327780°/117.874917° (4) Ecoregion: East Siberian taiga Test sample: shrubs classified as evergreen forest (SVM). Shrubs classified as river due to relief shadow. Based on the photo fund nearby, it is likely to be short evergreen forest. This is a reasonable confusion.	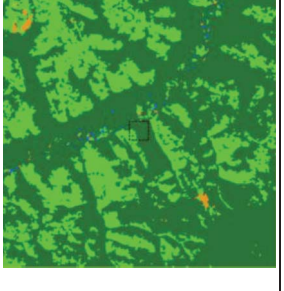	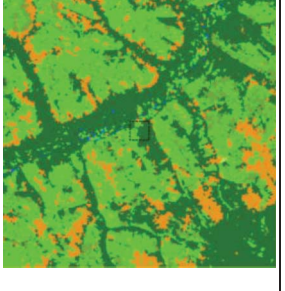
		40 classified as 22	40 classified as 63

Figure 16. Selected image samples from various part of the world where none of the classifiers classified correctly the test samples. From red to green are the poorest- to best-classified scenes in the central map. Indexed images are all taken from Google Earth with either screen captures of high-resolution satellite image snapshots or photographs taken in the field in the vicinity of our test samples. Curves are based on an annual time series of EVIs derived from MODIS

3	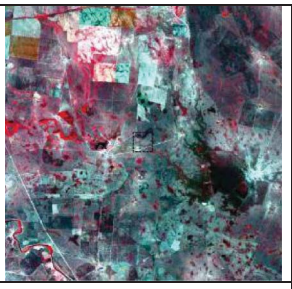	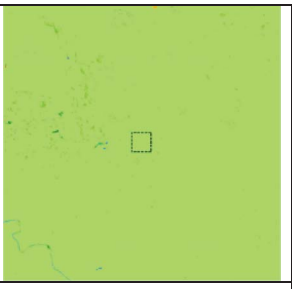	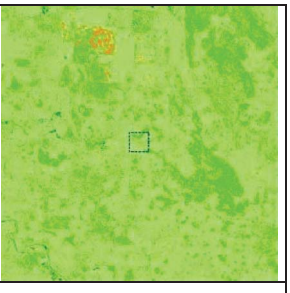
	(1) l5169025_02520090620 (2) Russia (3) Lat/Lon: 50.395167°/48.601947° (4) Ecoregion: Pontic steppe Test sample: natural grassland classified as bare cropland. This is a highly frequent mistake but spectrally difficult to distinguish. Involving texture features or field shapes could help reduce this confusion. RF seems to perform better in this case.	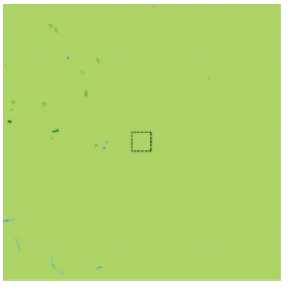	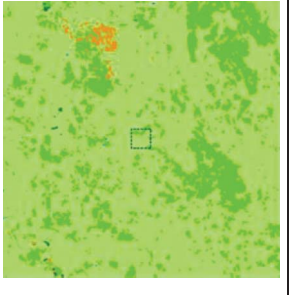
		32 classified as 94	32 classified as 94
4		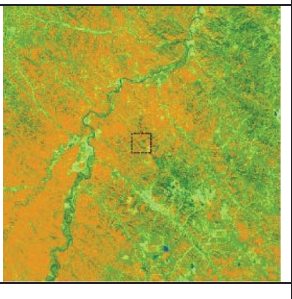	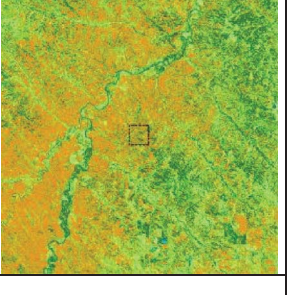
	(1) l5035029_02920100714 (2) USA (3) Lat/Lon: 44.863486°/–105.989086° (4) Ecoregion: Northern short grasslands Test sample: natural grassland classified as bare rock/gravel land. This is a frequent mistake due to low vegetation density and spectral mixing between grass and background soil.	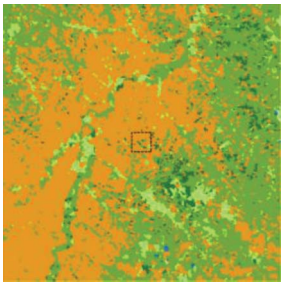	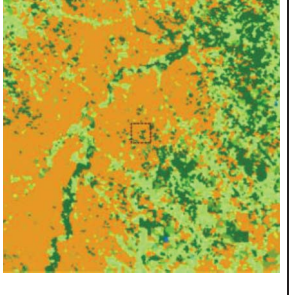
		32 classified as 93	32 classified as 93

Figure 16. (*Continued*). data for the entire year of 2010. The horizontal axes are from day 1 to day 365 of 2010, while the vertical axes are from 0.0 to 1.0. The centre of black boxes in the sample images mark the location of our test samples. The original image samples were displaying the near infrared, red, and green TM bands in red, green, and blue through some sort of greyscale stretching. The original classification results for the SVM and RF classifiers are shown in the same row with the original image but in the second and third columns, respectively. Corresponding to the original

.

5	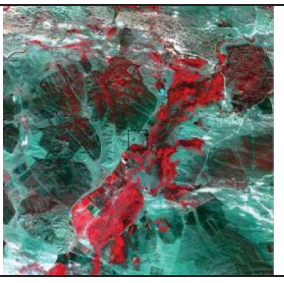	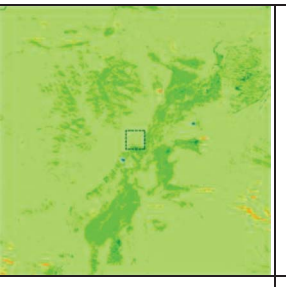	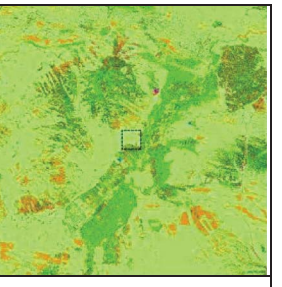
	(1) l5123030_03020100824 (2) China (3) Lat/Lon: 43.480413°/117.045839° (4) Ecoregion: Mongolian-Manchurian grassland Test sample: natural grassland classified as bare cropland. This is a difficult situation to use spectral data alone. RF seems to perform better here	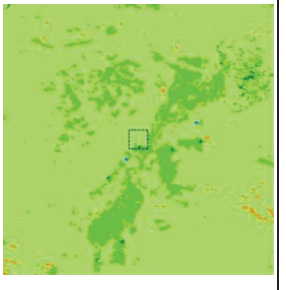	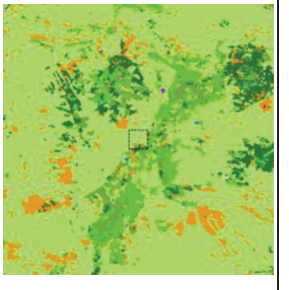
		32 classified as 93	32 classified as 93
6		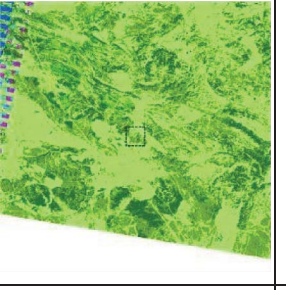	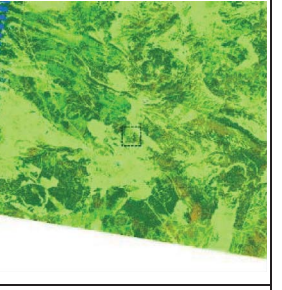
	(1) l5199032_03220090724 (2) Spain (3) Lat/Lon: 39.751953°/–1.882153° (4) Ecoregion: Iberian sclerophyllous and semi-deciduous forests Test sample: evergreen forest classified as shrubs. Mediterranean trees are sparse, therefore causing confusions. This could be improved by increasing training samples in this type of ecosystem.	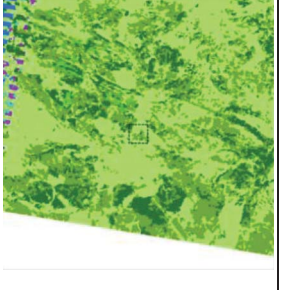	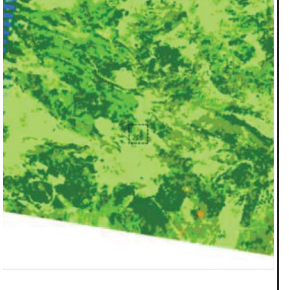
		22 classified as 40	22 classified as 40

Figure 16. (*Continued*). classification are the post-processed classification results through image segmentation and majority vote. The codes under the classification results were for level 2 land-cover types that can be found in Table 3.

7	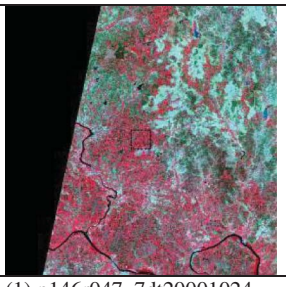	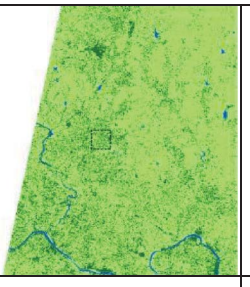	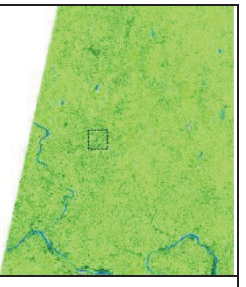
	(1) p146r047_7dt20001024 (2) India (3) Lat/Lon: 18.601120°/74.604309° (4) Ecoregion: Deccan thorn scrub forests Test sample: cropland classified as evergreen forest. This is a frequently made mistake in India. Cropland are mostly growing vegetable fields or fruit garden.	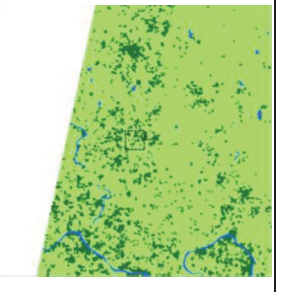	
		13 classified as 21	13 classified as 21
8		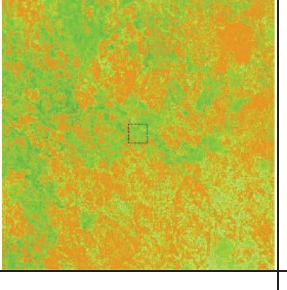	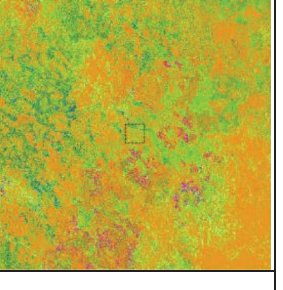
	(1) l5176053_05320091128 (2) Sudan (3) Lat/Lon: 10.570158°/26.919921° (4) Ecoregion: Sahelian Acacia savanna Test sample: shrubs classified as bare rock/gravel land. This is in a savanna area where shrubs, grass, and sparsely growing trees are intermixed. This confusion is reasonable.	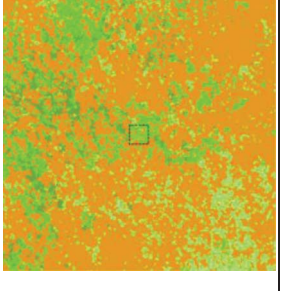	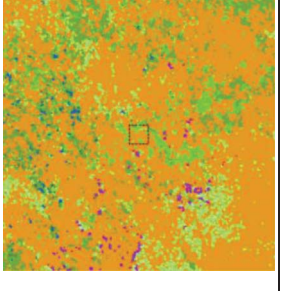
		40 classified as 93	40 classified as 93

Figure 16. (*Continued*).

Rocky Mountain areas in North America will be more thoroughly analysed and classified in our subsequent intensive mapping campaign. In Figure 16, we present extracted classification examples obtained with both SVM and RF classifiers. It can be seen that among the examples, the RF classifier tends to produce more diverse classification results than the SVM classifier. The reason behind it will be investigated in subsequent studies. We also displayed post-processed results through image segmentation. The post-processing that was

9	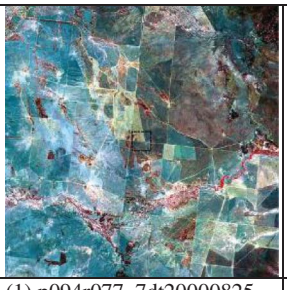	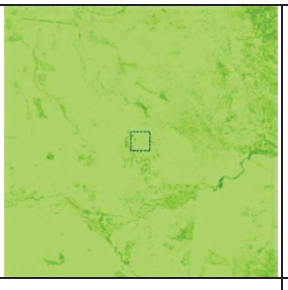	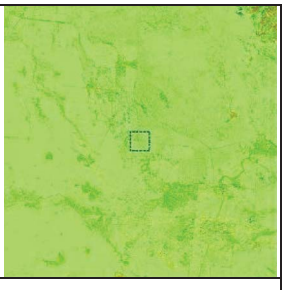
	(1) p094r077_7dt20000825 (2) Australia (3)Lat/Lon: –24.303039°/145.896405° (4) Ecoregion: Mitchell grass downs Test sample: shrub classified as bare cropland. This is a typical low-density shrub and grassland situation. Such confusion is spectrally difficult to distinguish but could be avoided using shape and texture features.		
		40 classified as 94	40 classified as 94
10		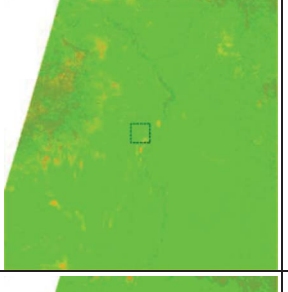	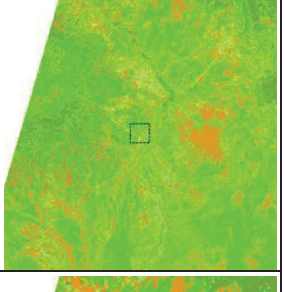
	(1) p228r090_7dt20000108 (2) Argentina (3) Lat/Lon: –42.559772°/–66.860920° (4) Ecoregion: Low Monte test sample: shrub classified natural grassland. This could be avoided perhaps by collecting sufficient number of samples.	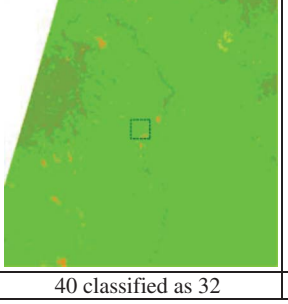	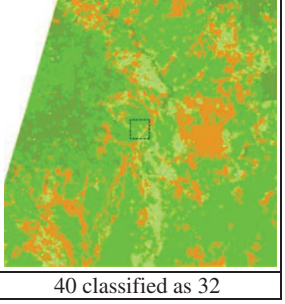
		40 classified as 32	40 classified as 32

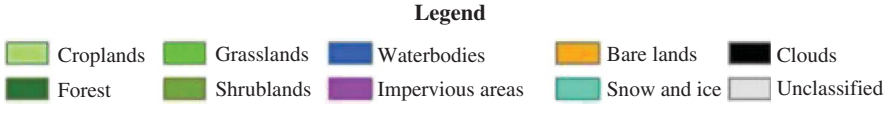

Figure 16. (*Continued*).

done based on segmentation with a scale set of 50 pixels (in general segments derived would be at least 50 pixels in size) removes the 'pepper and salt' effects. The results are useful to applications that are best met with polygon-based analysis (e.g. landscape ecological studies and biodiversity studies).

The initial goal of China's global land-cover mapping effort was to create a 30 m resolution land-cover product to address the needs of land surface process modelling (Verburg, Nevmann, and Nol 2011). Ge et al. (2007) subjected the regional atmospheric modelling system (RAMS), a regional land surface process model in Eastern Africa, to a sensitivity analysis with varying accuracies of land-cover data. They found when the accuracy of land-cover data was greater than 80%, the climate parameters modelled by the RAMS showed little sensitivity to the land-cover inputs. From this perspective, we are still 10–15% away from a desirable accuracy of land-cover products in order to support land surface process modelling efforts.

In this study, we only utilized six optical spectral bands. Spatial texture and temporal features have not been included. Ancillary data such as topography may also help improve classification accuracies. In addition, classification algorithms should be further tested. Since only classifiers were tested in this study, further improvement may be possible by (1) increasing the training data set size by pooling more samples from neighbourhood scenes; (2) allocating part of the test samples into the training; (3) pooling training data from within a basin or eco-region (Olthof et al. 2005); or (4) making use of object-based image analysis (Yu et al. 2006; Gamanya, de Maeyer, and deDapper 2007; Clinton et al. 2010).

Future efforts will be made to improve classification accuracies for croplands, shrubs, grasslands and particularly impervious surfaces whose accuracies are unacceptably low (Table 8). Although having accuracies around 20% is not uncommon in the land-cover classification community (Couturier 2010; Frey and Smith 2007), the impervious surface is poorly classified here with a barely 10.5% producer's accuracy and 30.8% user's accuracy. From a land-cover perspective, both croplands and grasslands are grass dominated. It is natural that they are heavily confused with each other. Morphologically and spectrally, all croplands, grasslands, and shrubs are similar during the growing season. Their confusions are also expected. While the vegetation is sparse, these classes are spectrally mixed with bare lands. On the other extreme, impervious surfaces are spectrally similar to barren lands. Nonetheless, shrublands and grasslands are heavily confused with forests and bare lands. Vegetation height information is likely to help differentiate these confused classes from forests and bare lands. Wetland and tundra were not considered as a level I class in this study. They are highly variable in space and time. Sulla-Menashe et al. (2011) suggest not considering wetland as a land-cover class as it is determined by the presence of water. Wetland should be extracted using ancillary data such as terrain and geomorphological data. Settlements and arid lands have been mapped globally with coarser resolution weather satellite data (Schneider, Friedl, and Potere 2010; Minoru et al. 2012). For 30 m resolution data, tundra should be classified with climate data. Both impervious surface and wetlands should be extracted with specially designed single-class extraction algorithms.

8. Conclusions and perspectives

Global land-cover mapping is a challenging task from almost every aspect of remote sensing, including data collection, geometric and atmospheric correction, mosaicking, feature extraction, classification, and accuracy assessment. Although a tremendous amount of research has been devoted to land-cover mapping with remotely sensed data, the present

capability in producing accurate land-cover maps over large areas with computers is far from satisfactory. A great number of image classification algorithms have been proposed but there is no general agreement on the best performers. It has been generally believed that not only do new algorithms need to be continuously developed (e.g. Xu et al. 2003; Yu et al. 2006; Liu et al. 2008) but more efforts should also be made to integrate the strengths of various classifiers (Clinton et al. 2009).

The initial results reported in this research for the first time compared four classification algorithms over the same type of data for the entire world and have consistently produced results in various parts of the world. The results have been placed in an open FTP site to ensure free use and further improvement by others (data.ess.tsinghua.edu.cn). There is a need for substantially more research in order to empirically determine geographic areas, feature types, and parameter settings, where various classifiers are strongest.

The research produced two distinctive sets of samples: 91,433 training samples and 38,664 test samples. This is an important source of data for global land-cover mapping. Because a majority of these samples were interpreted using ancillary high resolution imagery viewable from Google Earth, the quality of these two sample sets have high certainty. In addition, over 77% of the training samples and 38% of the test samples are large samples, greater than 500 m $\times$ 500 m in area. They are important references not only for our own research but also for mapping with coarser resolution data.

The finer resolution global land-cover map developed in this study provides opportunities for a large number of exciting future research projects. Our current effort only involved the spectral data in Landsat images. Future research could benefit from incorporating more features into the global land-cover classification (Franklin et al. 2011, Zurita-Milla et al. 2011) including lidar data (Huang et al. 2009; Hall et al. 2011), multi angular data (Selkowitz 2010), hyperspectral data (Xu and Gong 2007), and phenological data (Clark et al. 2010; Jeganathan, Dash, and Atkinson 2010). Second, it would be useful to investigate multitemporal land-cover classification using multiple Landsat images over the same area (Liu et al. 2008). Since there have been a large number of land cover data collected at the regional and local scales, they should be more comprehensively utilized to improve later global land-cover mapping efforts. Finally, more efforts should be made to extract individual land-cover categories, including agricultural and wetland areas using more specialized algorithms (e.g. Schneider et al. 2010; Zhong et al. 2011).

Acknowledgements

The authors are grateful to Anping Liao, Lijun Chen, Chaoying He, Dengsheng Lu, Damien Sulla-Menashe, Mark Friedl, Yanmei Yu, Peisheng Yan, Yan Jia, Hong Chen, Kang Jiang, Kai Yu, Dafei Yin, Na Cong, Vladimir Chakov, Viktorria Kuptcova, Li Jia, Liangzhi You, and John Townshend, who had assisted or advised them during various stages of this work. This research was partially supported by a National High Technology Grant from China (2009AA12200101) and a National Key Basic Research Programme of China (2010CB530300).

References

Adler-Golden, S. M., M. W. Matthew, L. S. Bernstein, R. Y. Levine, A. Berk, S. C. Richtsmeier, P. K. Acharya, G. P. Anderson, G. Felde, J. Gardner, M. Hoke, L. S. Jeong, B. Pukall, A. Ratkowski, and H.-H. Burke. 1999. "Atmospheric Correction for Short-Wave Spectral Imagery Based on MODTRAN4." *SPIE Proceedings, Imaging Spectrometry* 3753: 61–9.

Aksoy, S., K. Koperski, C. Tusk, and G. Marchis. 2009. "Land Cover Classification with Multi-Sensor Fusion of Partly Missing Data." *Photogrammetric Engineering and Remote Sensing* 75: 577–93.

Arino, O., P. Bicheron, F. Achard, J. Latham, R. Witt, and J. L. Weber. 2008. "GLOBCOVER the Most Detailed Portrait of Earth." *ESA Bulletin-European Space Agency* 136: 24–31.

Bartholomé, E., and A. S. Belward. 2005. "GLC2000: A New Approach to Global Land Cover Mapping from Earth Observation Data." *International Journal of Remote Sensing* 26: 1959–77.
Bauer, E., and R. Kohavi. 1998. "An Empirical Comparison of Voting Classification Algorithms: Bagging, Boosting, and Variants." *Machine Learning* 36: 1–38.
Bontemps, S., P. Defourney, E. Van Bogaert, and O. Arino. 2010. *GLOBCOVER2009 Products Description and Validation Report*. Accessed January 20, 2012. https://globcover.s3.amazonaws.com/LandCover2009/GLOBCOVER2009_Validation_Report_1.0.pdf.
Bounoua, L., R. Defries, G. J. Collatz, P. Sellers, and H. Khan. 2002. "Effects of Land Cover Conversion on Surface Climate." *Climatic Change* 52: 29–64.
Bradski, G. 2000. "The OpenCV Library." *Dr. Dobb's Journal of Software Tools* 25, no. 11: 120, 122–5.
Buchanan, G. M., A. Nelson, P. Mayaux, A. Hartley, and P. F. Donald. 2008. "Delivering a Global, Terrestrial, Biodiversity Observation System Through Remote Sensing." *Conservation Biology* 23: 499–502.
Carreiras, J. M. B., J. M. C. Preira, and Y. E. Shimabukuro. 2006. "Land-Cover Mapping in the Brazilian Amazon Using SPOT-4 Vegetation Data and Machine Learning Classification Methods." *Photogrammetric Engineering and Remote Sensing* 72: 897–910.
Caruana, R., and A. Niculescu-Mizil. 2006. "An Empirical Comparison of Supervised Learning Algorithms." In *Proceedings of the 23rd International Conference on Machine Learning*. Pittsburgh, PA.
Chang, C. C., and C. J. Lin. 2011. "LIBSVM: A Library for Support Vector Machines." *ACM Transactions on Intelligent Systems and Technology* 2: 27:1–27.
Chen, Y. L., and P. Gong. submitted. A Fast Unsupervised Classification Algorithm: Clustering Based on Eigen Space Transformation. *ISPRS Journal of Photogrammetry and Remote Sensing*.
Chuvieco, E., L. Giglio, and C. Justice. 2008. "Global Characterization of Fire Activity: Toward Defining Fire Regimes from Earth Observation Data." *Global Change Biology* 14: 1488–502.
Cihlar, J. 2000. "Land Cover Mapping of Large Areas from Satellites: Status and Research Priorities." *International Journal of Remote Sensing* 21: 1093–114.
Clark, M. L., T. M. Aide, H. R. Grau, and G. Riner. 2010. "A Scalable Approach to Mapping Annual Land Cover at 250 M Using MODIS Time Series Data: A Case Study in the Dry Chaco Ecoregion of South America." *Remote Sensing of Environment* 114: 2816–32.
Clinton, N., P. Gong, Z. Y. Jin, Z. Zhu, and B. Xu. 2009. "Meta-Prediction of *Bromus tectorum* Invasion in Central Utah, U.S.A." *Photogrammetric Engineering and Remote Sensing* 75: 689–701.
Clinton, N., C. Potter, B. Crabtree, V. Genovese, P. Gross, and P. Gong. 2010. "Remote Sensing Based Time Series Analysis of Cheatgrass (*Bromus techtorum* L.) Phenology." *Journal of Environmental Quality* 39: 955–63.
Couturier, S. 2010. "A Fuzzy-Based Method for the Regional Validation of Global Maps: The Case of MODIS-Derived Phenological Classes in a Mega-Diverse Zone." *International Journal of Remote Sensing* 31: 5797–811.
Cowardin, L. M. 1977. *Classification of Wetlands and Deep-Water Habitats of the United States*. Washington, DC: US Department of the Interior.
Dai, Y. J., X. Zeng, R. E. Dickinson, I. Baker, G. Bonan, M. Bosilovich, S. Denning, P. Dirmeyer, P. Houser, G. Niu, K. Oleson, A. Sclosser, and Z. L. Yang. 2003. "The Common Land Model." *Bulletin of American Meteorological Society* 84: 1013–23.
De Moraes, J. F. L., F. Seyler, C. C. Cerri, and B. Volkoff. 1998. "Land Cover Mapping and Carbon Pools Estimates in Rondonia, Brazil." *International Journal of Remote Sensing* 19: 921–34.
DeFries, R., C. Field, I. Fung, C. Justice, S. Los, P. Matson, E. Mathews, H. A. Mooney, C. S. Portter, K. Prentice, P. J. Sellers, J. R. G. Townshend, C. J. Tucker, S. L. Ustin, and P. M. Vitousek. 1995. "Mapping the Land-Surface for Global Atmosphere-Biosphere Models – Toward Continuous Distributions of Vegetations Functional-Properties." *Journal of Geophysical Research-Atmospheres* 100: 20867–82.
DeFries, R., J. R. G. Townshend, and M. Hansen. 1999. "Continuous Fields of Vegetation Characteristics at the Global Scale at 1-km Resolution." *Journal of Geophysical Research* 104, D14: 16911–23. doi:10.1029/1999JD900057.
DeFries, R. S., R. A. Houghton, and M. C. Hansen. 2002. "Carbon Emissions from Tropical Deforestation and Regrowth Based on Satellite Observations for the 1980s and 1990s."

Proceedings of the National Academy of Sciences of the United States of America 99: 14256–61.

Di Gregorio, A. 2005. *FAO Land Cover Classification System*. FAO Environment and Natural Resources Service Series, No. 8. Rome: FAO.

Dronova, I., L. Wang, and P. Gong. 2011. "Object-Based Analysis and Change Detection of Major Wetland Cover Types and Their Classification Uncertainty during the Low Water Period at Poyang Lake, China." *Remote Sensing of Environment* 115: 3220–36.

FAO. 2001. *FRA2000: Global Ecological Zoning for the Global Forest Resources Assessment 2000*, 200. Rome: FAO Forestry Department.

Foley, J. A., R. DeFries, G. P. Asner, C. Barford, G. Bonan, S. R. Carpenter, F. S. Chapin, M. T. Coe, G. C. Daily, J. H. M. Helkowski, T. Holloway, E. A. Howard, C. J. Kucharik, C. Monfreda, J. A. Patz, I. C. Prentice, N. Ramankutty, and P. K. Snyder. 2005. "Global Consequences of Land Use." *Science* 309: 570–4.

Foody, G. M. 2002. "Status of Land Cover Classification Accuracy Assessment." *Remote Sensing of Environment* 80: 185–201.

Franklin, S. E., Y. H. He, A. Pape, X. L. Guo, and G. J. Mcdermid. 2011. "Landsat-Comparable Land Cover Maps Using ASTER and SPOT Images: A Case Study for Large-Area Mapping Programmes." *International Journal of Remote Sensing* 32: 2185–205.

Frey, K. E., and L. C. Smith. 2007. "How Well Do We Know Northern Land Cover? Comparison of Four Global Vegetation and Wetland Products with a New Ground-Truth Database for West Siberia." *Global Biogeochemical Cycles* 21: GB1016.

Friedl, M. A., D. K. Mciver, J. C. F. Hodges, X. Y. Zhang, D. Muchoney, A. H. Strahler, C. E. Woodcock, S. Gopal, A. Schneider, A. Cooper, A. Baccini, F. Gao, and C. Schaaf. 2002. "Global Land Cover Mapping from MODIS: Algorithms and Early Results." *Remote Sensing of Environment* 83: 287–302.

Friedl, M. A., D. Sulla-Menashe, B. Tan, A. Schneider, N. Ramankutty, A. Sibley, and X. M. Huang. 2010. "MODIS Collection 5 Global Land Cover: Algorithm Refinements and Characterization of New Datasets." *Remote Sensing of Environment* 114: 168–82.

Fritz, S., L. See, and F. Rembold. 2010. "Comparison of Global and Regional Land Cover Maps with Statistical Information for the Agricultural Domain in Africa." *International Journal of Remote Sensing* 31: 2237–56.

Gamanya, R., P. De Maeyer, and M. De Dapper. 2007. "An Automated Satellite Image Classification Design Using Object-Oriented Segmentation Algorithms: A Move Towards Standardization." *Expert Systems with Applications* 32: 616–24.

Ganzeveld, L., L. Bouwman, E. Stehfest, D. P. Van Vuuren, B. Eickhout, and J. Lelieveld. 2010. "Impact of Future Land Use and Land Cover Changes on Atmospheric Chemistry–Climate Interactions." *Journal of Geophysical Research – Atmospheres* 115: D23301.

Ge, J., J. Qi, B. M. Lofgren, N. Moore, N. Torbick, and J. M. Olson. 2007. "Impact of Land Use/Cover Classification Accuracy on Regional Climate Simulations." *Journal of Geophysical Research* 112: D05107.

Giri, C., E. Ochieng, L. L. Tieszen, Z. Zhu, A. Singh, T. Loveland, J. Masek, and N. Duke. 2011. "Status and Distribution of Mangrove Forests of the World Using Earth Observation Satellite Data." *Global Ecology and Biogeography* 20: 154–9.

Gong, P. 2009a. "Assessment of Global Land Cover Map Accuracies Using Fluxnet Location Data." *Progress of Natural Sciences* 19: 754–9.

Gong, P. 2009b. "Some Frontier Problems in Remote Sensing Science and Technology." *Journal of Remote Sensing* 13: 16–28.

Gong, P., and P. J. Howarth. 1990. "An Assessment of Some Factors Influencing Multispectral Land-Cover Classification." *Photogrametric Engineering and Remote Sensing* 56: 597–603.

Gong, P., and P. J. Howarth. 1992a. "Land-Use Classification of SPOT HRV Data Using a Cover-Frequency Method." *International Journal of Remote Sensing* 13: 1459–71.

Gong, P., and P. J. Howarth. 1992b. "Frequency-Based Contextual Classification and Grey-Level Vector Reduction for Land-Use Identification." *Photogrametric Engineering and Remote Sensing* 58: 423–37.

Gong, P., J. R. Miller, and M. Spanner. 1994. "Forest Canopy Closure from Classification and Spectral Unmixing: A Multi-Sensor Evaluation of Application to an Open Canopy." *IEEE Transactions on Geoscience and Remote Sensing* 32: 1067–80.

Gong, P., Z. G. Niu, X. Cheng, K. Y. Zhao, D. M. Zhou, J. H. Guo, L. Liang, X. F. Wang, D. D. Li, H. B. Huang, Y. Wang, K. Wang, W. N. Li, X. W. Wang, Q. Ying, Z. Z. Yang, Y. F. Ye, Z. Li, D. F. Zhuang, Y. B. Chi, H. Z. Zhou, and J. Yan. 2010. "China's Wetland Change (1990–2000) Determined by Remote Sensing." *Science in China Series D (Earth Sciences)* 53: 1036–42.

Gong, P., Y. Sheng, and G. S. Biging. 2002. "3D Model-Based Tree Measurement from High Resolution Aerial Imagery." *Photogrammetric Engineering and Remote Sensing* 68: 1203–12.

Gong, P., Y. C. Zhao, L. Yu, and L. Liang. 2011. "Development of an Integrated Software Platform for Global Mapping and Analysis." *Geomatics World* 2: 34–7.

Hall, F. G., K. Bergen, J. B. Blair, R. Dubayah, R. Houghton, G. Hurtt, J. Kellndorfer, M. Lefsky, J. Ranson, S. Saatchi, H. H. Shugart, and D. Wickland. 2011. "Characterizing 3D Vegetation Structure from Space: Mission Requirements." *Remote Sensing of Environment* 115: 2753–75.

Hall, M., E. Frank, G. Holmes, B. Pfahringer, P. Reutemann, and I. H. Witten. 2009. "The WEKA Data Mining Software: An Update." *SIGKDD Explorations* 11: 10–18.

Hansen, M. C., R. DeFries, and J. Townshend. 2002. "Towards an Operational MODIS Continuous Field of Percent Tree Cover Algorithm: Examples Using AVHRR and MODIS Data." *Remote Sensing of Environment* 83: 303–19.

Hansen, M. C., R. S. DeFries, J. R. G. Townshend, and R. Sohlberg. 2000. "Global Land Cover Classification at 1 km Spatial Resolution Using a Classification Tree Approach." *International Journal of Remote Sensing* 21: 1331–64.

Herold, M., P. Mayaux, C. E. Woodcock, A. Baccini, and C. Schmullius. 2008. "Some Challenges in Global Land Cover Mapping: An Assessment of Agreement and Accuracy in Existing 1 km Datasets." *Remote Sensing of Environment* 112: 2538–56.

Hibbard, K., A. Janetos, D. P. Van Vuuren, J. Pongratz, S. K. Rose, R. Betts, M. Herold, and J. J. Feddema. 2010. "Research Priorities in Land Use and Land-Cover Change for the Earth System and Integrated Assessment Modelling." *International Journal of Climatology* 30: 2118–28.

Huang, C. Q., L. S. Davis, and J. R. G. Townshend. 2002. "An Assessment of Support Vector Machine for Land Cover Classification." *International Journal of Remote Sensing* 23: 723–49.

Huang, H., P. Gong, X. Cheng, N. Clinton, and Z. Li. 2009. "Improving Measurement of Forest Structural Parameters by Co-Registering of High Resolution Aerial Imagery and Low Density LiDAR Data." *Sensors* 9: 1541–58.

Imaoka, K., H. Fujii, H. Murakami, M. Hori, A. Ono, T. Igarashi, K. Nakagawa, T. Oki, Y. Honda, and H. Shimoda. 2010. "Global Change Observation Mission (GCOM) for Monitoring Carbon, Water Cycles, and Climate Change." *Proceedings of the IEEE* 98: 717–34.

Imhoff, M. L. 1997. "A Technique for Using Composite DMSP/OLS 'City Lights' Satellite Data to Map Urban Area." *Remote Sensing of Environment* 61: 361–70.

Jeganathan, C., J. Dash, and P. M. Atkinson. 2010. "Mapping the Phenology of Natural Vegetation in India Using a Remote Sensing-Derived Chlorophyll Index." *International Journal of Remote Sensing* 31: 5777–96.

Jung, M., K. Henkel, M. Herold, and G. Churkina. 2006. "Exploiting Synergies of Global Land Cover Products for Carbon Cycle Modeling." *Remote Sensing of Environment* 101: 534–53.

Knorn, J., A. Rabe, V. C. Radeloff, T. Kuemmerle, J. Kozak, and P. Hostert. 2009. "Land Cover Mapping of Large Areas Using Chain Classification of Neighboring Landsat Satellite Images." *Remote Sensing of Environment* 113: 957–64.

Lefsky, M. A. 2010. "A Global Forest Canopy Height Map from the Moderate Resolution Imaging Spectroradiometer and the Geoscience Laser Altimeter System." *Geophysical Research Letters* 37: L15401.

Liang, L., B. Xu, Y. L. Chen, Y. Liu, W. C. Cao, L. Q. Fang, L. M. Feng, M. F. Goodchild, and P. Gong. 2010. "Combining Spatial-Temporal and Phylogenetic Analysis Approaches for Improved Understanding on Global H5N1 Transmission." *PLoS ONE* 5: e13575.

Liu, D., M. Kelly, and P. Gong. 2006. "A Spatio-Temporal Approach to Monitoring Forest Disease Spread Using Multi-Temporal High Spatial Resolution Imagery." *Remote Sensing of Environment* 101: 167–80.

Liu, D. S., K. Song, J. R. G. Townshend, and P. Gong. 2008. "Using Local Transition Probability Models in Markov Random Fields in Forest Change Detection." *Remote Sensing of Environment* 112: 2222–31.

Liu, J. X., J. E. Vogelmann, Z. L. Zhu, C. H. Key, B. M. Sleeter, D. T. Price, J. M. Chen, M. A. Cochrane, J. C. Eidenshink, S. M. Howard, N. B. Bliss, and H. Jiang. 2011. "Estimating

California Ecosystem Carbon Change Using Process Model and Land Cover Disturbance Data: 1951–2000." *Ecological Modelling* 222: 2333–41.
Liu, M. 2007. *Atlas of China Physical Geography*, 254. Beijing: SinoMaps Press
Loveland, T. R., B. C. Reed, J. F. Brown, D. O. Ohlen, Z. Zhu, L. Yang, and J. W. Merchant. 2000. "Development of a Global Land Cover Characteristics Database and IGBP DISCover from 1 km AVHRR Data." *International Journal of Remote Sensing* 21: 1303–30.
Lu, D. S., H. Q. Tian, G. M. Zhou, and H. L. Ge. 2008. "Regional Mapping of Human Settlements in Southeastern China with Multisensor Remotely Sensed Data." *Remote Sensing of Environment* 112: 3668–79.
Mayaux, P., H. Eva, J. Gallego, A. Strahler, M. Herold, S. Agrawal, S. Naumov, E. Eduardo, C. M. Di Bella, C. Ordoyne, Y. Kopin, and P. S. Roy. 2006. "Validation of the Global Land Cover 2000 Map." *IEEE Transactions on Geoscience and Remote Sensing* 44: 1728–39.
Mccallum, I., M. Obersteiner, S. Nilsson, and A. Shvidenko. 2006. "A Spatial Comparison of Four Satellite Derived 1 km Global Land Cover Datasets." *International Journal of Applied Earth Observation and Geoinformation* 8: 246–55.
Neumann, M., L. Ferro-Famil, and A. Reigber. 2010. "Estimation of Forest Structure, Ground, and Canopy Layer Characteristics from Multibaseline polarimetric interferometric SAR Data." *IEEE Transaction on Geoscience and Remote Sensing* 40: 1086–104.
Niu, Z. G., P. Gong, X. Cheng, J. H. Guo, L. Wang, H. B. Huang, S. Q. Shen, Y. Z. Wu, X. F. Wang, X. W. Wang, Q. Ying, L. Liang, L. N. Zhang, L. Wang, Q. Yao, Z. Z. Yang, Z. Q. Guo, and Y. J. Dai. 2009. "Geographical Characteristics of China's Wetland Derived from Remote Sensing." *Science in China Series D (Earth Sciences)* 52: 723–38.
Olson, D. M., E. Dinerstein, E. D. Wikramanayake, N. D. Burgess, G. V. N. Powell, E. C. Underwood, J. A. D'amico, I. Itoua, H. E. Strand, J. C. Morrison, C. J. Loucks, T. F. Allnutt, T. H. Ricketts, Y. Kura, J. F. Lamoreux, W. W. Wettengel, P. Hedao, and K. R. Kassem. 2001. "Terrestrial Ecoregions of the World: A New Map of Life on Earth." *BioScience* 51: 933–8.
Olthof, I., C. Butson, and R. Fraser. 2005. "Signature Extension Through Space for Northern Landcover Classification: A Comparison of Radiometric Correction Methods." *Remote Sensing of Environment* 95: 290–302.
Potapov, P. V., S. A. Turubanova, M. C. Hansen, B. Adusei, M. Broich, A. Altstatt, L. Mane, and C. O. Justice. 2012. "Quantifying Forest Cover Loss in Democratic Republic of the Congo, 2000–2010, with Landsat ETM+ Data." *Remote Sensing of Environment* 122: 106–16.
Poulter, B., D. C. Frank, E. L. Hodson, and N. E. Zimmermann. 2011. "Impacts of Land Cover and Climate Data Selection on Understanding Terrestrial Carbon Dynamics and the CO(2) Airborne Fraction." *Biogeosciences* 8: 2027–36.
Powell, R. L., N. Matzke, C. De Souza, Jr., M. Clark, I. Numata, L. L. Hess, and D. A. Roberts. 2004. "Sources of Error in Accuracy Assessment of Thematic Land-Cover Maps in the Brazilian Amazon." *Remote Sensing of Environment* 90: 221–34.
Pu, R., Z. Li, P. Gong, I. Csiszar, R. Fraser, W. -M. Hao, S. Kondragunta, and F. Weng. 2007. "Development and Analysis of a 12-Year Daily 1-km Forest Fire Data across the North America from NOAA/AVHRR Data." *Remote Sensing of Environment* 108: 198–208.
Ramankutty, N., and J. A. Foley. 1998. "Characterizing Patterns of Global Land Use: An Analysis of Global Cropland Areas." *Global Biogeochemical Cycles* 12: 667–85.
Ramankutty, N., and J. A. Foley. 1999. "Estimating Historical Changes in Global Land Cover: Croplands from 1700 to 1992." *Global Biogeochemical Cycles* 13: 997–1027.
Roberts, D. A., M. Gardner, R. Church, S. Ustin, G. Scheer, and R. O. Green. 1998. "Mapping Chaparral in the Santa Monica Mountains Using Multiple Endmember Spectral Mixture Models." *Remote Sensing of Environment* 65: 267–79.
Running, S. W. 2008. "Ecosystem Disturbance, Carbon, and Climate." *Science* 321: 652–3.
Scepan, J. 1999. "Thematic Validation of High-Resolution Global Land-Cover Data Sets." *Photogrammetric Engineering and Remote Sensing* 65: 1051–60.
Schneider, A., M. A. Friedl, and D. Potere. 2010. "Mapping Global Urban Areas Using MODIS 500-M Data: New Methods and Datasets Based on 'Urban Ecoregions'." *Remote Sensing of Environment* 114: 1733–46.
Sedano, F., P. Gong, and M. Ferrao. 2005. "Land Cover Assessment with MODIS Imagery in Southern African Miombo Ecosystems." *Remote Sensing of Environment* 98: 429–41.
Selkowitz, D. J. 2010. "A Comparison of Multi-Spectral, Multi-Angular, and Multi-Temporal Remote Sensing Datasets for Fractional Shrub Canopy Mapping in Arctic Alaska." *Remote Sensing of Environment* 114: 1338–52.

Sheng, Y. W., C. A. Shah, and L. C. Smith. 2008. "Automated Image Registration for Hydrologic Change Detection in the Lake Rich Arctic." *IEEE Geoscience and Remote Sensing Letters* 5: 414–18.

Simard, M., N. Pinto, J. B. Fisher, and A. Baccini. 2011. "Mapping Forest Canopy Height Globally with Spaceborne Lidar." *Journal of Geophysical Research – Biogeosciences* 116: G04021.

Sterling, S. M., and A. Ducharne. 2008. "Comprehensive Data Set of Global Land Cover Change for Land Surface Model Applications." *Global Biogeochemical Cycles* 22: GB3017.

Sulla-Menashe, D., M. A. Friedl, O. N. Krankina, A. Baccini, C. E. Woodcock, A. Sibley, G. Q. Sun, V. Kharuk, and V. Elsakov. 2011. "Hierarchical Mapping of Northern Eurasian Land Cover Using MODIS Data." *Remote Sensing of Environment* 115: 392–403.

Tateishi, R., B. Uriyangqai, H. Al-Bilbisi, M. A. Ghar, J. Tsend-Ayush, T. Kobayashi, A. Kasimu, H. N. Thanh, A. Shalaby, B. Alsaaideh, T. Enkhzaya, G. Tana, and H. P. Sato. 2011. "Production of Global Land Cover, GLCNMO." *International Journal of Digital Earth* 4: 22–49.

Tchuenté, A. T. K., J. L. Roujean, and S. M. De Jong. 2011. "Comparison and Relative Quality Assessment of the GLC2000, GLOBCOVER, MODIS and ECOCLIMAP Land Cover Data Sets at the African Continental Scale." *International Journal of Applied Earth Observation and Geoinformation* 13: 207–19.

Thenkabail, P. S., C. M. Biradar, P. Noojipady, V. Dheeravath, Y. J. Li, M. Velpuri, M. Gumma, G. P. O. Reddy, H. Turral, X. L. Cai, J. Vithanage, M. Schull, and R. Dutta. 2009. "Global Irrigated Area Map (GIAM), Derived From Remote Sensing, for the End of the Last Millenium." *International Journal of Remote Sensing* 30: 3679–733.

Townshend, J. R. G., J. G. Masek, C. Q. Huang, E. F. Vermote, F. Gao, S. Channan, S. Jo, M. Feng, R. Narasimhan, D. Kim, K. Song, D. X. Song, X. P. Song, P. Noojipady, B. Tan, M. C. Hansen, M. X. Li, and R. E. Wolfe. 2012. "Global Characterization and Monitoring of Forest Cover Using Landsat Data: Opportunities and Challenges." *International Journal of Digital Earth* 5: 373–97.

Tucker, C. J., J. R. G. Townshend, and T. E. Goff. 1985. "African Land-Cover Classification Using Satellite Data." *Science* 227: 369–75.

Tuia, D., E. Pasoli, and W. J. Emery. 2011. "Using Active Learning to Adapt Remote Sensing Image Classifiers." *Remote Sensing of Environment* 115: 2232–42.

Verburg, P. H., K. Neumann, and L. Nol. 2011. "Challenges in Using Land Use and Land Cover Data for Global Change Studies." *Global Change Biology* 17: 974–89.

Wang, L., P. Gong, Q. Ying, Z. Yang, X. Cheng, and Q. Ran. 2010. "Settlement Extraction Over North China Plain with Landsat and Beijing-1 Data Using an Improved Watershed Segmentation Algorithm." *International Journal of Remote Sensing* 31: 1411–26.

Witten, I. H., and E. Frank. 2005. *Data Mining, Practical Machine Learning Tools and Techniques*, 525p. San Francisco, CA: Morgan Kaufmann Publishers.

Xu, B., and P. Gong. 2007. "Land Use/Cover Classification with Multispectral and Hyperspectral EO-1 Data." *Photogrammetric Engineering and Remote Sensing* 73: 955–65.

Xu, B., P. Gong, G. S. Biging, S. Liang, E. Seto, and B. Spear. 2004. "Snail Density Prediction for Schistosomiasis Control Using IKONOS and ASTER Images." *Photogrammetric Engineering and Remote Sensing* 70: 1285–94.

Xu, B., P. Gong, R. Spear, and E. Seto. 2003. "Comparison of Different Gray Level Reduction Schemes for a Revised Texture Spectrum Method for Land-Use Classification Using IKONOS Imagery." *Photogrammetric Engineering and Remote Sensing* 69: 529–36.

Yu, L., and P. Gong. 2012. "Google Earth as a Virtual Globe Tool for Earth Science Applications." *International Journal of Remote Sensing* 33: 3966–86.

Yu, Q., P. Gong, N. Clinton, G. Biging, and D. Schirokauer. 2006. "Object-Based Detailed Vegetation Mapping Using High Spatial Resolution Imagery." *Photogrammetric Engineering and Remote Sensing* 72: 799–811.

Zheng, Z., D. Mei, and E. Zhong. 2009. *Atlas of World Physical Geography*, 135. Beijing: Star Map Press.

Zhong, L. H., T. Hawkins, G. S. Biging, and P. Gong. 2011. "A Phenology-Based Approach to Map Crop Types in the San Joaquin Valley, California." *International Journal of Remote Sensing* 32: 7777–804.

Zurita-Milla, R. J., G. P. W. Clevers, J. A. E. Van Gijsel, and M. E. Schaepman. 2011. "Using MERIS Fused Images for Land-Cover Mapping and Vegetation Status Assessment in Heterogeneous Landscapes." *International Journal of Remote Sensing* 32: 973–91.